THE JOURNAL OF PHYSICAL CHEMISTRY C
A JOURNAL OF THE AMERICAN CHEMICAL SOCIETY

pubs.acs.org/JPCC

Article

Light-Induced Electron Paramagnetic Resonance Study of Charge Transport in Fullerene and Nonfullerene PBDB-T-Based Solar Cells

Victor I. Krinichnyi,* Evgeniya I. Yudanova, Nikolay N. Denisov, Aleksei A. Konkin, Uwe Ritter, Victor R. Bogatyrenko, and Alexander L. Konkin

Cite This: *J. Phys. Chem. C* 2021, 125, 12224−12240

Read Online

ACCESS | Metrics & More | Article Recommendations | Supporting Information

ABSTRACT: We present a combined light-induced electron paramagnetic resonance (LEPR) study of photoinitiation, relaxation, and recombination of charge carriers initiated by achromatic/white (with a color temperature of 5000 K) and monochromatic (with a photon energy of 1.34−3.41 eV) light in PBDB-T-based photovoltaic systems with $PC_{61}BM$, $PC_{71}BM$, and ITIC-M counterions. Charge carriers, polarons on polymer chains, and respective radical anions excited in disordered composite matrixes first fill spin traps, the number, energy depth, and spatial distribution of which are determined by the structure and crystallinity of bulk heterojunctions. By deconvolution of the effective LEPR spectra, the contributions of immobilized and mobile charge carriers, as well as their main magnetic resonance parameters, were determined separately at a wide variety of experimental conditions. The interaction of spins occupying different energy levels in the bandgap of a polymer semiconductor provokes the extreme photon energy sensitivity of the spin-assisted processes carried out in the polymer composites. The density functional theory calculations of the millimeter-waveband LEPR spectrum allowed the conclusion that polarons photoinitiated in the PBDB-T backbone are delocalized over its 4−5 monomers. Side $\pi-\pi$-stack packaging and *S*-isomerization of electron acceptors were also found. Predominant nongeminate recombination of charge carriers follows multistep trapping−detrapping spin hopping between sites of polymer layers and is strongly governed by the number, energy depth, and spatial distribution of spin traps. It was shown that all spin-involving processes in composites are spin-assisted and, therefore, are determined by the main magnetic resonance properties of both the spin charge carriers. The stability of charge carriers in a polymer-based composite was demonstrated to increase by more than an order of magnitude in the series of radical anions $PC_{61}BM^{-\bullet} \rightarrow$ ITIC-$M^{-\bullet} \rightarrow PC_{71}BM^{-\bullet}$. A further improvement in the functionality of the composite occurs at its slight 2,5-diphenyloxazole modification. The use of low-dimensional ITIC-M instead of PCBM and/or PPO with extended π-system significantly increases the exchange interaction between the spin charge carriers situated on the adjacent layers of the composite. This blocks intrachain charge diffusion but accelerates its interlayer hopping in the polymer matrix, which increases the efficiency and functionality of the composite.

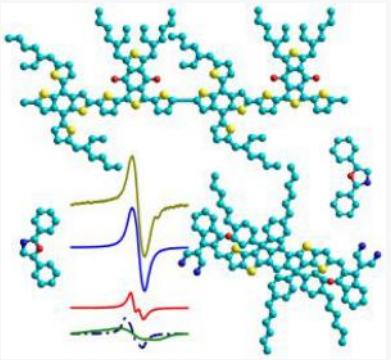

1. INTRODUCTION

Because fullerenes absorb only a part of the solar irradiation spectrum, the light power conversion efficiency (PCE) of respective polymer:fullerene bulk heterojunctions (BHJ) cannot reach high values.[1−3] This sparked the development and research of a new generation of nonfullerene electron-accepting molecules for more efficient organic photonics.[4] Among the new fullerene-free small molecular acceptors, the group of 3,9-bis(2-methylene-((3-(1,1-dicyanomethylene)-6/7-methyl)-indanone))-5,5,11,11-tetrakis(4-hexylphenyl)-dithieno[2,3-d:2′,3′-d′]-s-indaceno[1,2-b:5,6-b′]dithiophene (ITIC-M in Figure 1) and its derivatives is one of the most representative compounds exhibiting desirable power conversion efficiency (PCE) in conjunction with some electron donating polymers. Currently, PCE of 6.8−15.6% was reached for a lot of different ITIC-based solar cells with poly[(2,6-(4,8-bis(5-(2-ethylhexyl)thiophen-2-yl)benzo[1,2-b:4,5-b′]-dithiophene)-*co*-(1,3-di(5-thiophene-2-yl)-5,7-bis(2-ethylhexyl)benzo[1,2-c:4,5-c′]dithiophene-4,8-dione)] (PBDB-T in Figure 1) electron-donating matrix,[5−8] e.g., 12.2% for PBDB-T:ITIC-M composite.[9] However, despite successful use of such BHJ in photovoltaics, studies of their charge transport properties remain scarce and vary greatly.[5,10−14]

Excitons photoinitiated in a photovoltaic composite tend either to dissociate into pairs of cations and anions with the rate constant k_d or to relax to the ground state with the other rate constant k_r. The former stage is accompanied by the formation of oppositely charged polarons $P^{+\bullet}$ (holes) on polymer chains and radical anions $A^{-\bullet}$ (free electrons)

Received: April 16, 2021
Revised: May 11, 2021
Published: May 25, 2021

https://doi.org/10.1021/acs.jpcc.1c03427
J. Phys. Chem. C 2021, 125, 12224−12240

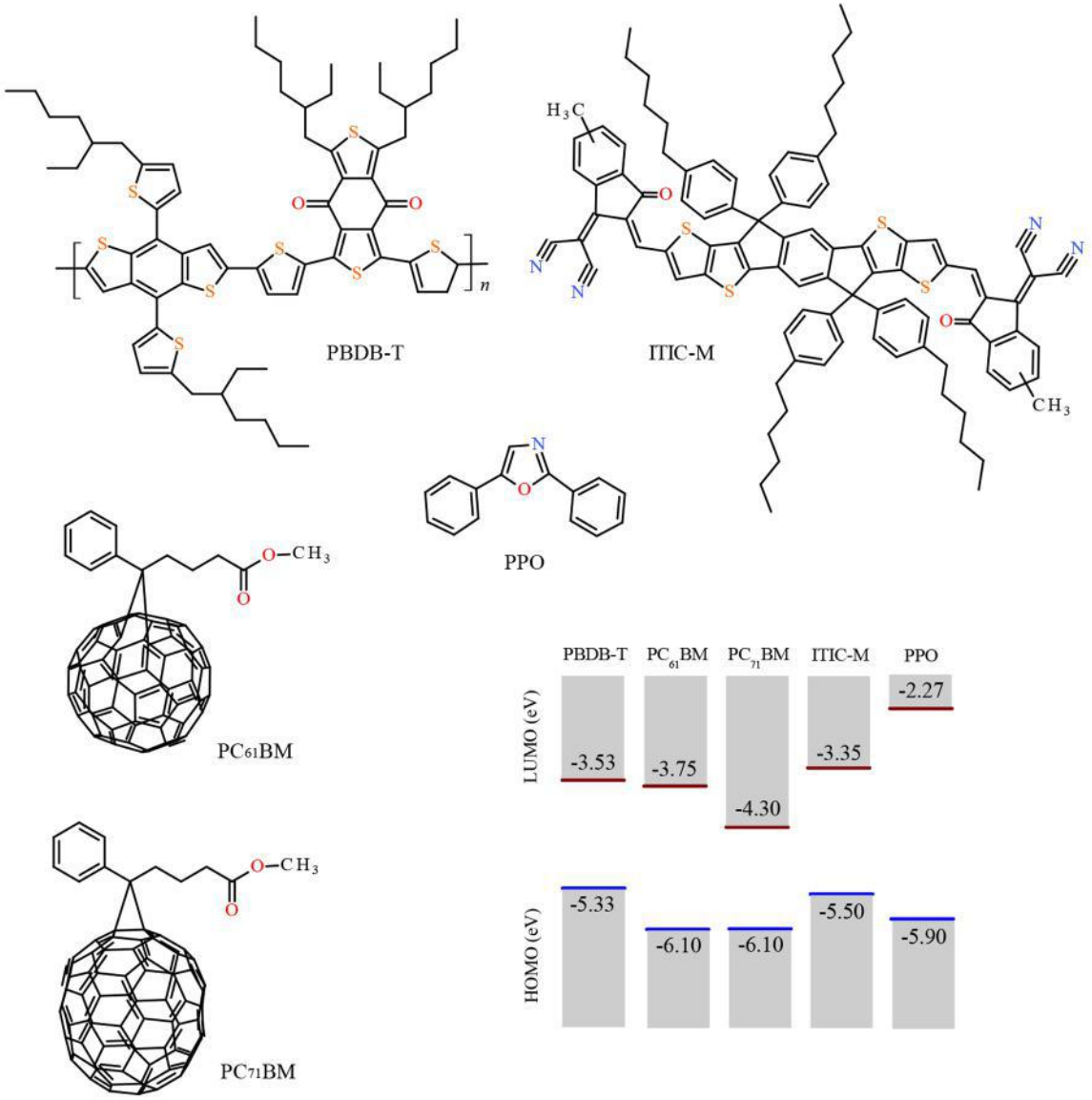

Figure 1. Schematic structures of PBDB-T, $PC_{61}BM$, $PC_{71}BM$, ITIC-M, and PPO used for preparation of polymer composites. Below the LUMO and HOMO energy level diagrams obtained for each material used in the study are shown schematically.[6,34−36]

possessing spin $S = {}^1/_2$. If k_d exceeds k_r, only a limited number of these carriers, proportional to the difference $k_d - k_r$, should be able to transfer the charges toward the corresponding electrodes. The residual number of charge carriers can be additionally reduced due to the capture of their part by high-energy spin traps formed in the composite matrix due to its structural disordering. Upon sample illumination, these traps are first filled with free charge carriers, which then indirectly participate in all processes carrying out in the composite. So then, only a small fraction of free charges formed as a result of exciton dissociation able to leave BHJ and reach electrodes. The paramagnetic nature of charge carriers determines the spin-assistant character of all processes occurring in such systems. These processes become dependent not only on the structure and morphology of a sample but also on the number, energetic depth, and spatial distribution of spin traps in its BHJ as well as on the energy and density of the initiated phonons.[15] For their accurate identification and control, it is very important to obtain correlations between the spin states of charge carriers and molecular/structural/morphological properties of these systems. Therefore, the spin state, composition, and dynamics of all charge carriers are an important task. Because both the opposite charge carriers possess spin $S = {}^1/_2$, direct light-induced electron paramagnetic resonance (LEPR) spectroscopy appeared to be the most effective and suitable method for detailed investigation of spin-assisted processes carried out in various organic polymer[16−18] and copolymer[19−22] systems. For example, charge separation and recombination photoinitiated in BHJ formed by poly[2,6-(4,4-bis(2-ethylhexyl)-4*H*-cyclopenta[2,1-b;3,4-b′]-dithiophene)-*alt*-4,7-(2,1,3-benzothiadiazole)] (C-PCPDTBT), its analogues, and [6,6]-phenyl-C_{61}-butanoic acid methyl ester ($PC_{61}BM$) were studied by using the time-resolved EPR (TR-EPR) method.[23] It has shown drastic (more than two orders of magnitude) acceleration of electron relaxation of polarons at Si modification of this composite. Such effect was attributed to different concentrations of spin traps in the C-PCPDTBT:$PC_{61}BM$ and Si-PCPDTBT:$PC_{61}BM$ BHJ. LEPR

https://doi.org/10.1021/acs.jpcc.1c03427
J. Phys. Chem. C 2021, 125, 12224−12240

study of the ITIC-modified PBDB-based polymers has shown a decisive spin-dependent role in the formation and recombination of charge carriers.[24] The energy of excited photons was found to effect weakly the effective/isotropic *g*-factor of charge carriers excited in the PBDB-T:ITIC BHJ. At the 3 mm/84 GHz waveband spin echo EPR, a weak anisotropy of the *g*-factors and the line widths of polarons and counterions photoinitiated in the composite PBDB-T:ITIC was studied, and the main tensor values of these magnetic resonance parameters were evaluated.[25] It should be noted, however, that the relaxation times of charge carriers determined by pulse EPR in some conjugated polymers[26−28] and polymer:fullerene composites[23,29] appeared to be more than 1−2 orders of magnitude slower than those determined by continuous wave (cw) EPR technique. Such discrepancy in the data obtained by pulse and cw methods can be due to a fundamental limitation inherent in the pulsed EPR technique, namely its deadtime around 100 ns, which prevents the registration of paramagnetic centers with very short relaxation times. Normally, these parameters of mobile charge carriers freely diffusing in organic photovoltaic systems are too short and therefore cannot be registered by pulse EPR methods.

There should exist various factors leading to high energy-conversion efficiency of nonfullerene composites with PBDB-T and analogous backbones. Among them, it can be lamellar ordering due to a more planar counterion and/or optimized band structure and, therefore, a stronger $\pi-\pi$-coupling in these systems. The distinctive $\pi-\pi$ molecular packing plays a key role in the process of charge transfer in organic donor−acceptor systems. Such molecular ordering accelerates a delocalization of electron wave functions at donor:acceptor interfaces that significantly reduce the Coulomb attraction between interfacial electron−hole pairs. Important is the fact that lamellar structure is characteristic not only for molecular single crystals[30] but also for BHJ of some thin films.[8,31] The exchange interaction of spin carriers was shown[21,22] to improve electronic properties of organic donor−acceptor systems, similar to how it happens in inorganic anisotropic layered 2D-systems,[32] and therefore should indeed play a decisive role in charge transport through their BHJ. However, the effect of the structural features of nonfullerene electron acceptors on the resulting morphology of respective composites is not yet understood. Photophysics underlying the relaxation, dynamics, and other spin-dependent processes occurring in this and analogous compounds has been studied in fragments, remain ambiguous, and has not been solved completely. In a previous study, it was shown[33] that addition of a small amount of 2,5-diphenyloxazole (PPO) or 1,2-benzopyrone (BP) molecules to the thiophene-based photovoltaic composite additionally improves the morphology and functional properties of this system. Such additives were suggested to be considered as the structure/crystallization mediating centers of the composite matrix, by analogy with the boiling/crystallization centers in superheated/supercooled liquids. One would expect a similar process to be implemented, e.g., in PBDB-T-based composite in which small planar ITIC-M and/or PPO molecules can act as structural mediators.

We report here the results of a detailed cw LEPR study of spin-assisted processes of excitation, separation, relaxation, dynamics, and recombination of charge carriers photoinitiated in BHJ formed by PBDB-T and ITIC-M at a wide range of photon energies. These results were compared with those obtained for the PBDB-T:ITIC-M BHJ slightly doped with PPO molecules as well as for the PBDB-T:$PC_{61}BM$ and PBDB-T:[6,6]-phenyl-C_{71}-butanoic acid methyl ester ($PC_{71}BM$) composites. Use of the direct magnetic resonance method allowed us to reveal the spin assistance of magnetic, relaxation, and dynamics parameters of spin charge carriers photoinitiated in this system to identify their dynamics and recombination in BHJ and also to reveal the selectivity of these parameters to the photon energy. The effect of PPO doping and dimension of counterions on spin-assisted processes in PBDB-T-based BHJ is discussed. The results obtained by LEPR spectroscopy are compared to those evaluated from the density functional theory (DFT) calculations.

2. EXPERIMENTAL SECTION

2.1. Materials Used in Experiments. In this work, the following were used: poly[(2,6-(4,8-bis(5-(2-ethylhexyl)-thiophen-2-yl)benzo[1,2-b:4,5-b′]dithiophene)-*co*-(1,3-di(5-thiophene-2-yl)-5,7-bis(2-ethylhexyl)benzo[1,2-c:4,5-c′]-dithiophene-4,8-dione)] (PBDB-T in Figure 1) distributed by the Ossila Ltd., UK, [6,6]-phenyl-C_{61}-butanoic acid methyl ester ($PC_{61}BM$ in Figure 1) distributed by the Solenne BV, The Netherlands, [6,6]-phenyl-C_{71}-butanoic acid methyl ester ($PC_{71}BM$ in Figure 1) distributed by the Solenne BV, The Netherlands, 3,9-bis(2-methylene-((3-(1,1-dicyanomethylene)-6/7-methyl)-indanone))-5,5,11,11-tetrakis(4-hexylphenyl)-dithieno[2,3-d:2′,3′-d′]-s-indaceno[1,2-b:5,6-b′]-dithiophene (ITIC-M in Figure 1) distributed by the Ossila Ltd., UK, and 2,5-diphenyloxazole (PPO in Figure 1) distributed by Aldrich, United States. Figure 1 demonstrates the molecular energy-level diagrams of all ingredients used in the study with the lowest unoccupied molecular orbital (LUMO) and highest occupied molecular orbital (HOMO) energy levels, E_{LUMO} and E_{LUMO}, respectively.[6,34−36]

2.2. Preparation of the Samples. Samples were prepared as follows. First, 25 mg of the PBDB-T was dissolved in 1.25 mL of chlorobenzene. The resulting solution was sonicated in a DADI DA-968 50 W ultrasonic bath for 10 min and heated at T = 323 K for 10 min to achieve complete dissolution. Solutions of the $PC_{61}BM$, $PC_{71}BM$, and ITIC-M acceptors in chlorobenzene with a concentration of 20 mg/mL were prepared separately. Each of these solutions was mixed with a treated polymer solution to obtain a concentration of 10 mg/mL for each respective ingredient. The solutions obtained in this manner were heated at T = 325 K for 30 min, then cast by 5 μL drops on both surfaces of the corresponding ceramic plates, and completely dried in an inert atmosphere. As a result of this procedure, 0.85 mg of the corresponding composite was placed on both sides of these plates. A part of the PBDB-T:ITIC-M sample obtained was additionally doped with PPO up to 6 wt % by adding to its solution a respective quantity of PPO molecules according to a procedure described earlier.[33] Finally, all of the samples were heated at T = 433 K for 30 min before LEPR experiments.

2.3. NIR-Vis-UV Absorption Spectra of Composites. Optical absorption spectra of the polymer composites were obtained at T = 298 K by using the spectrophotometer Specord-250-plus (Analytik Jena), which was able to scan within the band 1.13−6.53 eV (1100−190 nm). They are shown fully in Figure S1 of the Supporting Information. The composition and positions of the spectral components were determined accurately by using the differentiation of experimental absorption spectra.

https://doi.org/10.1021/acs.jpcc.1c03427
J. Phys. Chem. C 2021, 125, 12224−12240

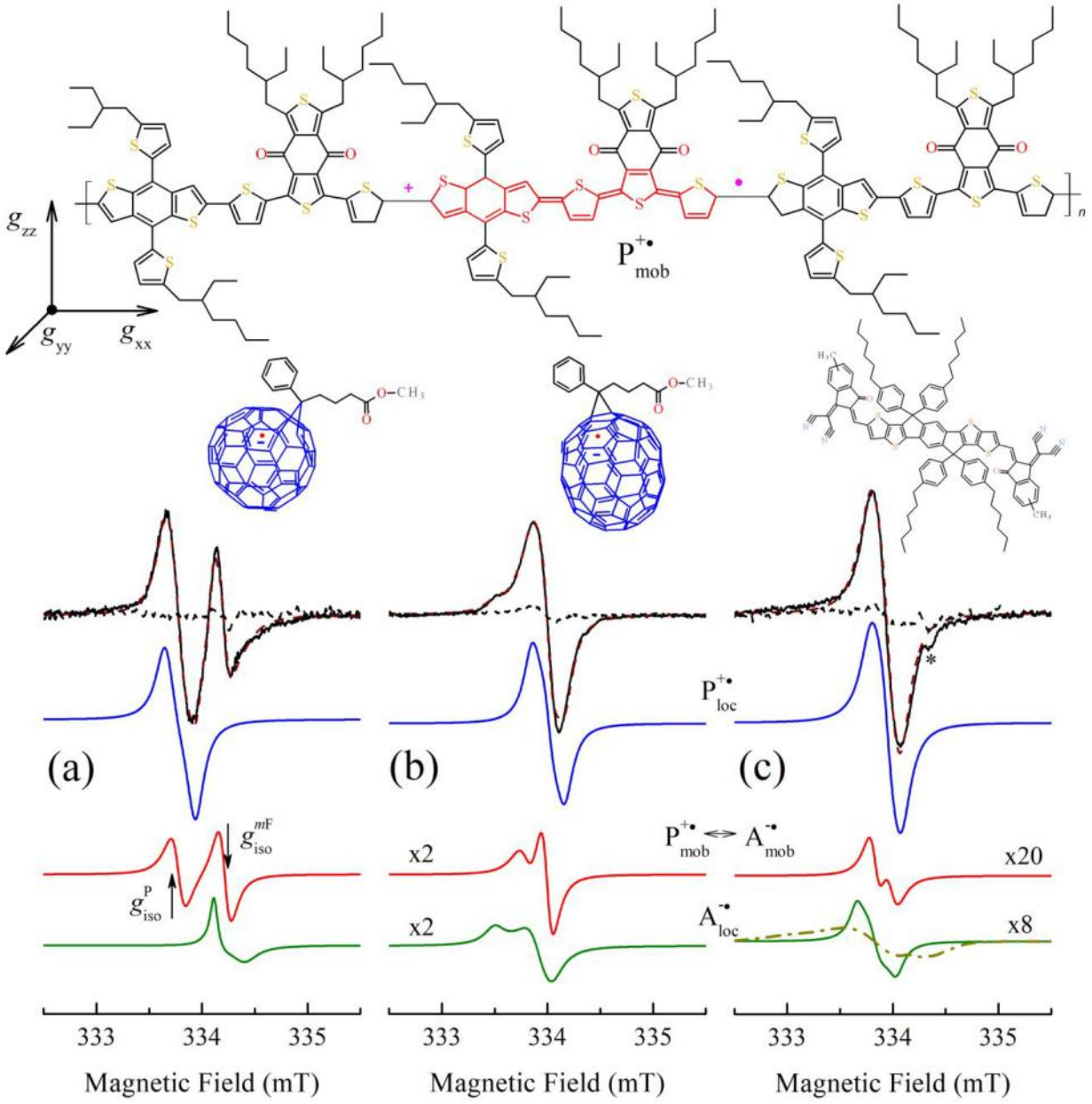

Figure 2. X-band (9.5 GHz, 334 mT) effective LEPR spectra of charge carriers background excited in the PBDB-T:$PC_{61}BM$ (a), PBDB-T:$PC_{71}BM$ (b), and PBDB-T:ITIC-M (c) composites at T = 77 K by achromatic white light with CCT of T_c = 5000 K. Appropriate experimental spectra of the darkened samples and calculated sum spectra EPR are shown by dashed lines. The weak asterisk-marked line in (c) can be attributed to defects in the polymer backbone. Lorentzian LEPR spectra best fitting the effective experimental ones with their contributions caused by polarons stabilized in the PBDB-T, $P^{+\bullet}$, these carriers immobilized in spin traps of a copolymer matrix, $P^{+\bullet}_{loc}$, respective counter radical anions $A^{-\bullet}_{loc}$ ($A^{-\bullet}$ = $PC_{61}BM^{-\bullet}$, $PC_{71}BM^{-\bullet}$, and ITIC-$M^{-\bullet}$) as well as highly mobilized pairs of radicals, $P^{+\bullet}_{mob} \leftrightarrow A^{-\bullet}_{mob}$, illuminated by white light with CCT of T_c = 5000 K using the parameters summarized in Table 1 are also shown. Spectral contributions of the PBDB-T:ITIC-M composite shown in (c) were calculated by using the terms of g-factor obtained for polarons localized in the PBDB-T matrix.[25] However, when calculating these terms, the hfc of their spin charge carriers with surrounding hydrogen nuclei should also be taken into account (dash-dotted line, see Section 3.4 and Supporting Information, Section VI). On the top are schematically shown the structures of BHJ formed in the respective polymer nanocomposites and mobile polaron $P^{+\bullet}_{mob}$ excited in their polymer matrixes. The spin of the real quasi-particle occupies a larger ($n \geq 5$) number of copolymer monomers than shown in the Figure (see Section 3.4). The orientation of the principal axes of the polaron's **g**-tensor is also given. In (a) are shown the positions of the contributions of mobile polarons $P^{+\bullet}_{mob}$ and methanofullerene radical anions $PC_{61}BM^{-\bullet}_{mob}$ as an example.

2.4. Excitation of Spin Charge Carriers. Initial excitons and subsequent spin charge carriers were generated as a result of the steady-state irradiation of composites by the LED-based light sources with the photon energy/wavelength, $h\nu_{ph}/\lambda_{ph}$, bands of 1.34−3.41/923−364 eV/nm through a short quartz light guide directly in the MW cavity of the EPR spectrometer. The experimental conditions were preoptimized as described in the Supporting Information, Section II. Irradiation spectra of the LEDs used in experiments were measured by the Optofiber FSD-9 spectrometer equipped with a computer-controlled 16-bit analog-digital convertor. The light energy of the LEDs came through a quartz light guide on the spectrometer's sensor in the same manner as in the case of LEPR experiments. The luminous emittance I_{LED} values of the sources were determined

https://doi.org/10.1021/acs.jpcc.1c03427
J. Phys. Chem. C 2021, 125, 12224−12240

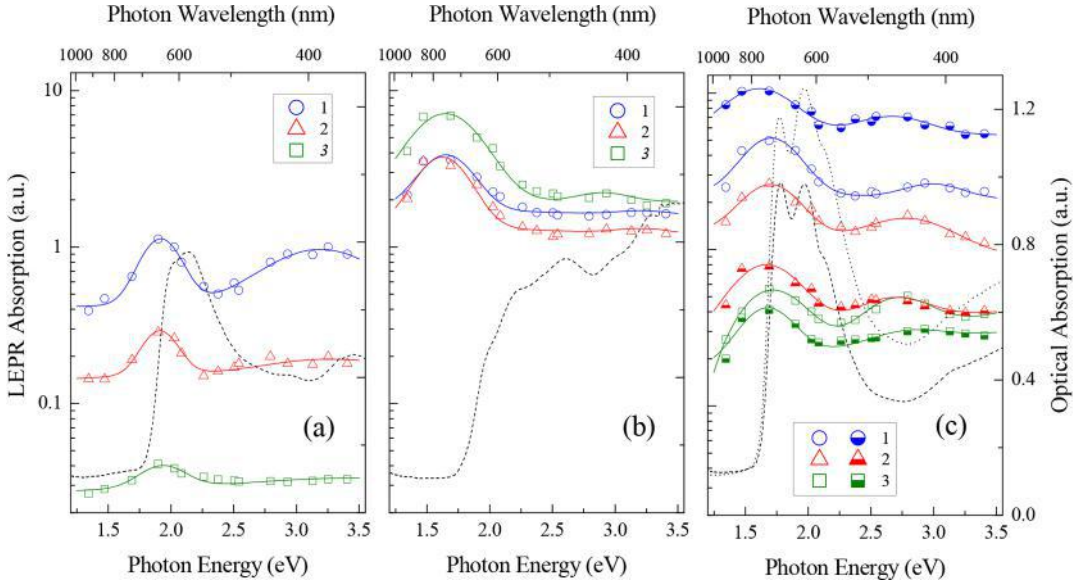

Figure 3. LEPR absorbance by localized polarons PBDB-T$^{+\bullet}$ (1), mobile polarons and radical anions A$^{-\bullet}$ (2), and immobilized radical anions A$^{-\bullet}$ (3) photoinitiated in the (a) PBDB-T:$PC_{61}BM$ (A$^{-\bullet}$ = $PC_{61}BM^{-\bullet}$), (b) PBDB-T:$PC_{71}BM$ (A$^{-\bullet}$ = $PC_{71}BM^{-\bullet}$), (c) PBDB-T:ITIC-M (open points, A$^{-\bullet}$ = ITIC-M$^{-\bullet}$) and PBDB-T:ITIC-M/$PPO_{0.06}$ (semifilled points, A$^{-\bullet}$ = ITIC-M$^{-\bullet}$) composites at T = 77 K by photons with different frequency/wavelength, $h\nu_{ph}/\lambda_{ph}$. The solid lines are drawn arbitrarily only for illustration to guide the eye. A low-energy part of NIR-Vis-UV absorption spectra of the PBDB-T:$PC_{61}BM$, PBDB-T:$PC_{71}BM$, and PBDB-T:ITIC-M samples fully shown in Figure S1 are depicted by dashed lines, whereas such spectrum obtained for the PBDB-T:ITIC-M/$PPO_{0.06}$ sample is depicted by dotted line.

using the IMO-2N broadband light emission power meter with thermocouple-based sensor and LX-1010BS digital luxmeter and were used for further normalization of the number of spins photoinitiated in the composites under study.

2.5. LEPR Spectra Measurements and Processing. All of the samples were studied by using cw EPR X-band (B_0/ν_e = 3340 mT/9.7 GHz) PS-100.X spectrometer with a maximum microwave power of 150 mW and 100 kHz phase synchronous detection. Dark and photoinduced LEPR spectra of electron donor−acceptor nanocomposites shown in Figure 2 were obtained at 77 K by being inserted into a quartz Dewar filled with liquid nitrogen and placed into the center of the EPR spectrometer cavity. For EPR measurements at T = 90−320 K, the sample was placed in another quartz flow Dewar cell and centered in a stream of dry nitrogen, whose temperature was stabilized by the BRT SKB IOC controller with a platinum temperature sensor pt100 in its feedback loop. The room temperature spectrum of polarons excited in the solution of PBDB-T in dichorobenzene was recorded for its further DFT simulation using a Bruker K-band spectrometer ELEXYS E500 operated at 24 GHz in magnetic field B_0 = 860 mT according to an earlier described procedure.[37] The signal-to-noise ratio of LEPR spectra was improved by their accumulation during their multiple scans. Spectral contribution and concentration of different spin ensembles were determined by decomposition of effective EPR spectra registered far from their MW saturation and in combination with the "light on-light off" procedure described earlier.[19,38,39] Landé g-factors of spin charge carriers were determined using the *N*,*N*-diphenyl-N′-picrylhydrazyl (DPPH) standard with g = 2.0036 ± 0.0002.[40] The processing and simulation of experimental EPR spectra were performed using the EasySpin[41] and OriginLab software. LEPR spectra were simulated using the splitting $g_{xx} - g_{yy} = 1 \times 10^{-3}$ and $g_{yy} - g_{zz} = 3 \times 10^{-4}$ obtained for polarons photoinitiated in the PBDB-T:ITIC BHJ.[25] The accuracy of estimating the intensity I, g-factor of the line, and the distance between its positive and negative spectral peaks ΔB_{pp} was determined to be 5%, $\pm 2 \times 10^{-4}$ and $\pm 2 \times 10^{-3}$ mT, respectively. The calculation of hyperfine coupling parameters of the PBDB-T:ITIC-M system was performed using the method/functional/basis sets (DFT/B3LYP/6-311G) in Gaussian-2016 and (B3LYP-) in ORCA according a procedure earlier described in detail.[22] The preliminary molecular energy minimization and structure optimization have been carried out in Chem3D by MM2 force field method. The spin−lattice T_1 and spin−spin T_2 relaxation times of spin charge carriers were determined with an accuracy of 7.7% and 1.5%, respectively, using the steady-state MW saturation method,[42] adapted for the study of spin pairs photoinitiated in organic donor−acceptor nanocomposites[43] (see Supporting Information, Section III).

3. RESULTS AND DISCUSSION

3.1. NIR-Vis-UV Absorption Spectra of Copolymer Composites. The resulting NIR-vis-UV spectra of the composites studied are shown partly in Figure 3 and fully together with the initial materials in Figure S1 of the Supporting Information. They consist of band contributions of polaron P$^{+\bullet}$ in the PBDB-T matrix and respective electron-donating radical anions A$^{-\bullet}$ situated between polymer chains. The spectrum of the PBDB-T polymer contains bands registered at 2.03/611, 2.14/579, 3.44/360, and 4.96/250 eV/nm. The shoulder registered at 2.03/612 eV/nm appears to be due to the effect of intermolecular aggregation.[10] The nonfullerene acceptor ITIC-M contributes to the sum absorption spectrum of the main bands at 1.77/701, 1.93/642, 4.49/276, and 6.26/198 eV/nm. In the longer waveband, it exhibits well-defined absorption peaks with a vibronic shoulder, which indicates the presence in the films of ordered aggregation and strong $\pi-\pi$-stacking interaction.[44] This counterion adds to the spectrum the bands registered at 6.26/198 and 4.49/276 eV/nm as well as a strong wideband extending from ca. 1.55/800 to 2.48/500 eV/nm with a central

https://doi.org/10.1021/acs.jpcc.1c03427
J. Phys. Chem. C 2021, 125, 12224−12240

peak situated at near 1.77/700 eV/nm attributed to the HOMO π−LUMO π^* transition.[6] Modification of the polymer with a methanofullerene acceptor $PC_{61}BM$ leads to the appearance in the spectrum of the corresponding composite of a line at 2.94/422 eV/nm of a fullerene set band[45,46] as well as to a change in the shape of the long-wavelength peak situated at ca. 2.07/600 eV/nm. So, the entire set of composite bands contains contributions situated at 2.01/617, 2.14/579, 2.94/422, 3.46/358, and 4.98/249 eV/nm. The effective spectrum of the PBDB-T:$PC_{71}BM$ composite consists of the separate bands recorded at 1.78/696, 1.97/629, 2.14/579, 4.54/273, and 5.21/238 eV/nm. Methanofullerene $PC_{71}BM$ contributes to this spectrum a side fullerene band situated at 5.21/238 eV/nm[10] as well as a shoulder recorded at 1.78/696 eV/nm, which is a characteristic feature of the donor−acceptor interaction between the polymer backbone and fullerene globes during charge transfer between them. The PBDB-T:ITIC-M composite is characterized by a set of the main bands situated at 1.77/701, 1.97/629, 2.14/579, 4.59/270, and 5.21/238 eV/nm. The lateral band at 1.77/701 eV/nm indicates the presence of an ITIC-M acceptor, while the adjacent band 1.97/629 eV/nm indicates the donor−acceptor interaction of the counterions with the polymer backbone. When this composite is lightly doped with the small molecule PPO, approximately the same set of its characteristic main bands remains. In this case, the optical density of the ultraviolet region of the total spectrum of the modified composite increases due to the addition to it of the specific PPO band.

3.2. LEPR Spectral Composition and Magnetic Resonance Parameters. The pristine fullerene derivatives and ITIC-M do not exhibit any noticeable EPR signals even upon their illumination by photons within the whole energy region used in experiments. Shadowed polymer:fullerene BHJ may demonstrate weak LEPR signal attributed either to intrinsic paramagnetic defects or to charge carriers excited by IR phonons irradiated by internal active elements of the EPR spectrometer.[33] Such signals arising in EPR spectra of the PBDB-T:$PC_{61}BM$, PBDB-T:$PC_{71}BM$, and PBDB-T:ITIC-M composites are shown in Figure 2 by respective dashed lines. Figure 1 shows that the HOMO level of PBDB-T is the highest one of all the other adductive materials. This allows excitons generated in the polymer backbone to migrate to BHJ formed by this donor with all the acceptors used and then dissociate there into free electrons and holes, respectively. Figure 2 depicts experimental exemplary LEPR spectra of the samples illuminated by white (T_c = 5000 K) light at T = 77 K directly in the MW cavity. Indeed, the background light illumination of the samples leads to the sharp increase in their LEPR signals, as is shown in Figure 2. As in the case of other similar composites,[19] such signal growth is explained by the formation of oppositely charged mobile polarons $P^{+\bullet}_{mob}$ on polymer chains and radical anions $A^{-\bullet}_{mob}$ = $PC_{61}BM^{+\bullet}_{mob}$, $PC_{71}BM^{+\bullet}_{mob}$, ITIC-$M^{+\bullet}_{mob}$ embedded into polymer backbone, as shown schematically at the top of Figure 2. Because an unpaired electron delocalized along a polaron weakly interacts with the *S* and *O* heteroatoms incoming into the PBDB-T backbone, it provokes rhombic symmetry of its density. The strong interaction of an unpaired electron with such heteroatom nuclei normally leads to a significant increase in their Landé splitting parameter g.[47,48] Because the effective EPR spectra of all samples studied are recorded around a magnetic field characteristic of a free electron with the Landé factor g_e = 2.00232, one can conclude the realization of a weak interaction in their BHJ. Nevertheless, this interaction provokes a weak anisotropy of g-factors, other main magnetic resonance parameters of polarons, and radical anions photoinitiated in these and other polymer composites. This becomes most obvious when recording LEPR spectra in the millimeter wavebands, in which a higher spectral resolution is achieved.[16,20,49] The values of these parameters of mobile/free charge carriers are averaged due to their fast dynamics. Normally, it can be polaron diffusion in a polymer backbone and/or vibration/libration of radical anions $A^{-\bullet}$ situated between polymer chains. For example, the main values of their **g**-tensors are averaged shifting to an effective (isotropic) g-factor, $g_{iso} = {}^1/_3(g_{xx} + g_{yy} + g_{zz})$. Spin dynamics averages the other magnetic resonant parameters analogously. Therefore, the effective LEPR spectra of the composites presented in Figure 2 should contain spectral contributions from paramagnetic centers with different natures, concentrations, and dynamics. To study all processes occurring in the composites with the above charge carriers, one should first divide their contributions into effective LEPR signals and determine magnetic, resonance, and dynamic parameters of these charge carriers. It can be made from deconvolution of the initial LEPR spectra using the "light on−light off" procedure.[38,39,50] Effective LEPR spectra shown in Figure 2 and their contributions due to the polarons $P^{+\bullet}_{loc}$ captured by spin traps, immobilized radical anions $A^{-\bullet}_{loc}$, and mobile quasi-pairs $P^{+\bullet}_{mob} \leftrightarrow A^{-\bullet}_{mob}$ (here $A^{-\bullet}$ = $PC_{61}BM^{-\bullet}$, $PC_{71}BM^{-\bullet}$, and ITIC-$M^{-\bullet}$) calculated with the data summarized in Table 1 are also presented. As in the case of other copolymers,[22,39] the principal x-axis of $P^{+\bullet}_{mob}$ carriers was chosen to be parallel to the longest polymer c-axis, whereas the y-axis lies in the thiophene plane, and the z-axis is directed perpendicular to x- and y-axes. It can be seen from Figure 2a that the better spectral resolution (ca. 0.4 mT) is achieved for the contributions of mobile polarons $P^{+\bullet}_{mob}$ and C_{60}-based radical anions due to the highest distance between their spectra with appropriate g_{iso} located at a smaller and larger magnetic field, respectively. The deconvolution of the spectra allowed us to obtain separately the above-mentioned magnetic resonance parameters of localized and mobile charge carriers, photoinitiated in the composites under study at a wide range of experimental conditions.

Table 1. Main Values of g- and ΔB_{pp}-tensors Used for Simulation of Donor−Acceptor Contributions of the LEPR Spectra[a]

parameters	PBDB-$T^{+\bullet}$	$PC_{61}BM^{-\bullet}$	$PC_{71}BM^{-\bullet}$	ITIC-$M^{-\bullet}$	ITIC-$M^{-\bullet}$/$PPO_{0.06}$
g_{xx}	2.00327	2.00038	2.00545	2.00401	2.00403
g_{yy}	2.00224	2.00028	2.00289	2.00304	2.00299
g_{zz}	2.00146	1.99865	2.00212	2.00190	2.00196
g_{iso}	2.00232	1.99977	2.00349	2.00298	2.00299
ΔB^x_{pp}, mT	0.144	0.103	0.149	0.156	0.157
ΔB^y_{pp}, mT	0.154	0.081	0.236	0.170	0.173
ΔB^z_{pp}, mT	0.134	0.097	0.144	0.156	0.157
ΔB^{iso}_{pp}, mT	0.144	0.094	0.176	0.161	0.162

[a]Notes: For the simulations were used the splitting $g_{xx} - g_{yy} = 1 \times 10^{-3}$ and $g_{yy} - g_{zz} = 3 \times 10^{-4}$ obtained for polarons localized in the PBDB-T matrix.[25] The actual line width should be normalized with the coefficient $\delta \approx 0.6$−0.7 (see the text).

3.3. Paramagnetic Susceptibility. Figure 3 depicts the equal scaled dependences of concentrations of all charge

https://doi.org/10.1021/acs.jpcc.1c03427
J. Phys. Chem. C 2021, 125, 12224−12240

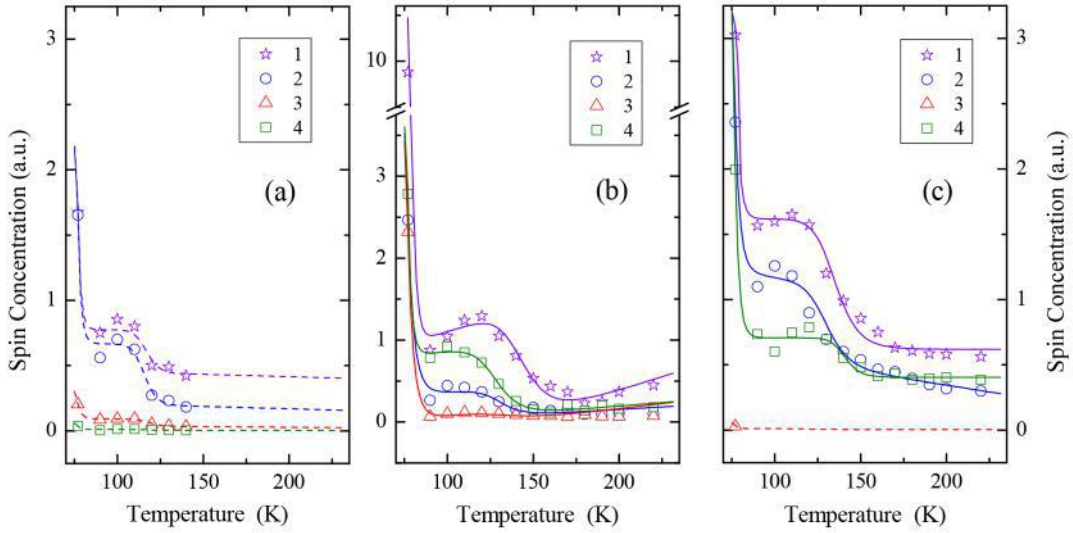

Figure 4. Temperature dependences of effective spin concentration and its contributions due to mobile and immobilized charge carriers photoinitiated by white light with T_c = 5000 K in the PBDB-T:$PC_{61}BM$ (a), PBDB-T:$PC_{71}BM$ (b), and PBDB-T:ITIC-M (c) composites. Dashed lines show the dependences calculated from eq 1 with respective parameters summarized in Table 2.

carriers photoinitiated in the PBDB-T:$PC_{61}BM$, PBDB-T:$PC_{71}BM$, and PBDB-T:ITIC-M composites as a function of the photon energy $h\nu_{ph}$ obtained at T = 77 K. For the comparison, the IR-vis-UV absorption spectra of respective samples are also shown. From the analysis of the data presented in Figure 3, the following conclusions can be made. The first of them is the obvious dependence of the number of charge carriers on the origin of composites studied and photon energy. One can note the prevalence of charge carriers localized in BHJ of all these samples and also the dependence of spin concentration on the phonon energy. It is seen that both the mobile and localized charge carriers excited in the PBDB-T:$PC_{61}BM$ sample demonstrate concentration dependence with extrema at phonon energies around 1.9 and 3.2 eV. These values obtained for the other samples decrease down to ca. 1.7 and 2.9 eV. The left-situated extremum is recorded around the energy of the bandgap of the polymer backbone, $\Delta E_g = E_{HOMO} - E_{LUMO}$ = 1.80 eV,[6] whereas the other extremum appears at the higher photon energies. A similar effect was also manifested when studying charge carriers photoinitiated in different photovoltaic composites[15,22,51,52] and was explained to arise due to the interaction of captured charge carriers with the light photons and neighboring paramagnetic centers. Replacing the $PC_{61}BM$ acceptor with the ITIC-M one in the composite leads to a significant, more than an order of magnitude, increase in the number of all spin charge carriers. A further increase in the sum spin concentration and in its fraction due to the methanofullerene radical anions occurs in the PBDB-T:$PC_{71}BM$ composite. This behavior correlates with a decrease in the energy bandgap $\Delta E_g = E_{HOMO} - E_{LUMO}$ of respective anions in these samples from 2.35 first to 2.15 and then to 1.80 eV. This is also consistent with the change in the integral number of the light quanta evaluated from their IR-vis-UV spectra shown in Figure 3. So, the number of detrapped polarons should depend on the energetic depth and spatial distribution of spin traps, the polymer bandgap, and the energy of exiting photons. Once these energies become roughly the same, a larger number of localized polarons tends to leave the traps and become mobile. This accelerates charge transfer across the donor−acceptor boundary of a composite.

The better functional properties of PBDB-T:ITIC composites described in the literature can be due to their lamellar structure and/or planarity of the ITIC molecules jointly causing a stronger $\pi-\pi$-coupling of electron-donating and electron-accepting subsystems and, therefore, their optimized band structure. Previously, it was shown[33] that the introduction of a small amount of planar PPO molecules with extended π-system into a polymer:fullerene composite significantly improves its functional properties. It would be appropriate to notice that in the study of colloidal series of Pb-containing perovskites,[53] a significant increase in the photoluminescent quantum yield of such systems was recorded upon adding a certain amount of PPO. This effect was explained by surface orbitals' hybridization of nitrogen atoms in PPO molecules and Pb atoms of perovskites due to their exchange interaction. The analogous interaction could be expectably realized between PPO, PBDB-T, and ITIC-M molecules in the PBDB-T:ITIC-M/$PPO_{0.06}$ composite. During the doping, they can easily be incorporated between the chains of the composite matrix and the ITIC-M molecules. This promotes a greater overlap of their molecular $\pi-\pi$-orbitals and the formation of intermolecular van der Waals bonds between the composite subsystems. The proximity of E_{LUMO} of all the composite subsystems should provoke nonradiative energy transfer between them. This transfer can be significantly accelerated due to the existence of additional sublevels E_{LUMO+1} and E_{LUMO+4} of nitrogen atoms of PPO molecules.

To clarify the factor affecting the functional properties of the PBDB-T-based systems, the PBDB-T:ITIC-M composite doped with small PPO molecules to a level of 6 wr% was correspondingly studied. Figure 3c also depicts the dependence of respective LEPR and optics absorption signals of the PBDB-T:ITIC-M/$PPO_{0.06}$ composite on the photon energy $h\nu_{ph}$. It is seen from the data presented that the modification of the initial sample PBDB-T:ITIC-M with PPO molecules has little effect on the intensity and position of the above-mentioned extrema. On the other hand, the doping leads to a more than twofold increase in the concentration of all spin

https://doi.org/10.1021/acs.jpcc.1c03427
J. Phys. Chem. C 2021, 125, 12224−12240

Table 2. Parameters ΔE_{ij}, ν^0_{hop}, and E_a[a]

anion	parameter	PBDB-T$^{+\bullet}$/A$^{-\bullet}$	PBDB-T$^{+\bullet}_{loc}$	A$^{-\bullet}_{mob}$	A$^{-\bullet}_{loc}$
$PC_{61}BM^{-\bullet}$	ΔE_{ij}, eV	0.331	0.312	0.248	0.268
	ν^0_{hop}, s^{-1}	5.1×10^{19}	5.8×10^{19}	4.9×10^{19}	5.6×10^{19}
	E_a, eV	0.159	0.158	0.161	0.165
$PC_{71}BM^{-\bullet}$	ΔE_{ij}, eV	0.274	0.161	0.188	0.281
	ν^0_{hop}, s^{-1}	6.22×10^{16}	2.21×10^{17}	2.73×10^{13}	9.78×10^{16}
	E_a, eV	0.112	0.117	0.024	0.106
ITIC-M$^{-\bullet}$	ΔE_{ij}, eV	0.254	0.202		0.210
	ν^0_{hop}, s^{-1}	2.24×10^{17}	2.11×10^{17}		3.79×10^{18}
	E_a, eV	0.121	0.115		0.161

[a]Evaluated from eq 1 for spin charge carriers initiated in the PBDB-T-based composites by photons of white light with T_c = 5000 K.

charge carriers photoinitiated in PPO-modified BHJ. It would also be important to note that such a modification of the donor−acceptor composite provokes a significant reduction in the number of mobile carriers after.

The balance of the initiation and recombination of the charge carriers depends expectable also on temperature. Figure 4 shows temperature dependences of sum concentrations of all spin charge carriers as well as their contributions due to mobile and immobilized polarons and respective radical anions photoinitiated in the BHJ under study by white light with T_c = 5000 K. These parameters are also proportional to the difference $k_d - k_r$ which is governed by molecular and order properties of the composites. As can be seen from Figure 4a, the concentrations of the above paramagnetic centers photoinitiated in the PBDB-T:$PC_{61}BM$ sample sharply decrease to minimum values when the temperature increases up to 140 K. At the higher temperatures, the accuracy of registration of these radicals decreases due to low signal-to-noise ratio. The analogous dependencies are registered also for charge carriers in other samples, which are characterized with the higher difference $k_d - k_r$ (see Figure 4b,c). The appearance in these curves of the stair-like term around temperature region of 100−130 K is also seen. Similar dependences were previously recorded in the study of poly(3-hexylthiophene):$PC_{71}BM$[51] and a series of narrow band gap composites.[22,33] They can be interpreted as follows.

According to the Miller−Abrahams tunneling model,[54] polarons diffusing between initial i and final j sites of a single polymer chain spend the difference of their energies ΔE_{ij}. In a real polymer system, its exchange interaction with the other spins leads to the higher overlapping of their π-orbits and redistribution of spin density between neighboring polymer chains that should also be taken into account.[55,56] The amplitude of such interaction is determined mainly by the average spin density on each polymer unit and the rate of spin intrachain diffusion with the expenditure of energy ΔE_{ij}. Generally, the relation for the effective paramagnetic susceptibility of polarons with spin $S = {}^1/_2$ can be written as[57−59]

$$\chi(\Delta E_{ij}, E_a) = \chi_0 \frac{2(1+\alpha^2)}{\alpha^2} \exp\left(\frac{\Delta E_{ij}}{k_B T}\right) \quad (1)$$

where χ_0 is a proportional constant, $\alpha = ({}^3/_2)J_{ex}/h\nu_{hop}$, J_{ex} is the amplitude of spin exchange during their collision and intrachain hopping diffusion with the rate $\nu_{hop} = \nu^0_{hop}\exp(-E_a/k_BT)$, ν^0_{hop} is a prefactor, k_B is the Boltzmann constant, and h is the Plank constant. The appearance of the stair-like term in Figure 4 indicates a stronger and weaker exchange interaction of the spins situated on neighboring polymer chains at lower and higher temperatures, respectively. The dependences calculated from eq 1 with ΔE_{ij}, ν^0_{hop}, and E_a presented in Table 2 and J_{ex} = 0.021 eV are also shown in Figure 4. These curves are shown to approximate well the data obtained experimentally for all samples. This allows the conclusion in this and analogous systems of spin tunneling within the framework of the Miller−Abrahams model in parallel with their intrachain hopping, which depends on spin traps and also on their exchange interaction with the nearest spin ensembles. One should, however, take into account a possible initial formation in the composites of pairs of localized oppositely charged polarons $P^{+\bullet}_{loc} \leftrightarrow P^{-\bullet}_{loc}$ with equal energy and g-factors[60] and diamagnetic bipolarons which are able to dissociate into spin polaron couples, $BP^{2+} \leftrightarrow 2P^{+\bullet}$.[61−63] The combination of these processes could also initiate the appearance of the above-mentioned term in the temperature dependences obtained.

The analysis of the data presented in Figures 3 and 4 allows us to conclude that the better planarity of PPO counterions enhances spin $\pi-\pi$-interaction of polarons formed on neighboring chains and prevents their recombination with the nearest counterions. Slight doping of the polymer matrix with small planar molecules increases additionally the interaction of spins situated on the nearest layers. This even more increases the stability of charge carriers, shifts the equilibrium of their formation and recombination processes, and thereby increasing their LEPR signals, so then sum concentration of mobile and immobilized spin charge carriers in the composite series PBDB-T:$PC_{61}BM$ → PBDB-T:ITIC-M → PBDB-T:ITIC-M/$PPO_{0.06}$ → PBDB-T:$PC_{71}BM$ increases 1.0 → 3.8 → 8.2 → 10.1 times, respectively. At the same time, $\pi-\pi$-interaction reduces the relative amount of mobile charge carriers photoinitiated in the samples. This assumption also confirms the data shown in Figures S3 and S5 and summarized in Table S1 of the Supporting Information. This can be explained by the confinement of polarons[64,65] due to the enhancement of interchain coupling. Polaron confinement provokes faster binding and/or recombination of mobile charge carriers and rather interchain/interlayer charge transfer between localized polarons than its intrachain diffusion by mobile spin carriers.[66] In this case, the density of the preferable charge transfer between polarons immobilized on neighboring polymer layers should increase in the series of composites PBDB-T:$PC_{61}BM$ → PBDB-T:$PC_{71}BM$ → PBDB-T:ITIC-M → PBDB-T:ITIC-M/$PPO_{0.06}$ (see Figures 3 and 4). This correlates well with the spin density excited on each polymer unit of these composites equal to 0.23, 0.36, 0.67, and 0.86, respectively, at steady-state illumination by white light with T_c = 5000 K.

https://doi.org/10.1021/acs.jpcc.1c03427
J. Phys. Chem. C 2021, 125, 12224−12240

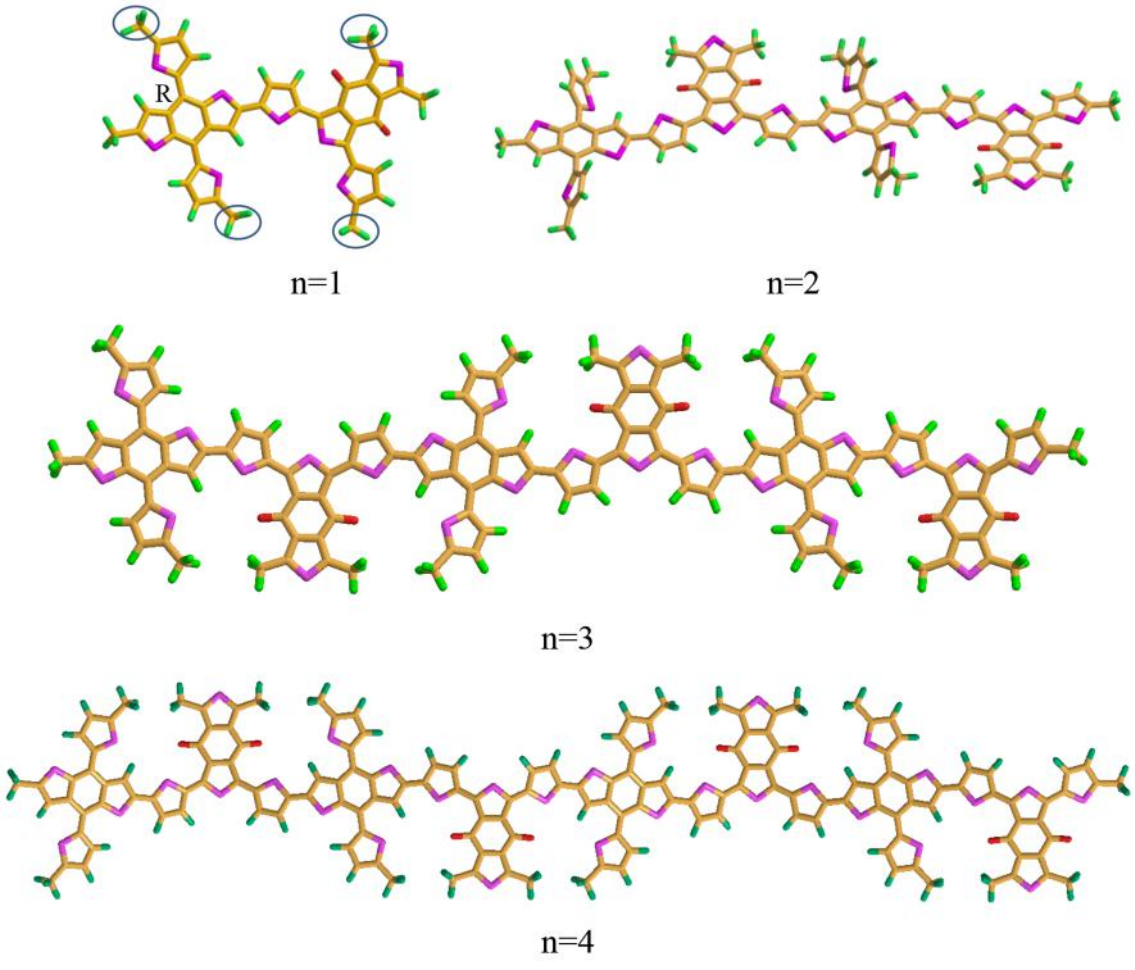

Figure 5. *n*-BDB-T oligomers with n = 1−4 used for hfc (or SDD) evaluation.

3.4. DFT Evaluation of PBDB-T Oligomers and ITIC-M ^{1}H Hyperfine Coupling. Among the numerous EPR applications to organic solar cell (OSC) composites, the consideration of the hyperfine coupling (hfc) of electron−nuclear spins in photogenerated radical ions is certainly in focus of the study. This coupling is characterized by a constant $A_{hfc} = Q_\rho$, where Q is the McConel constant and ρ is spin density on the OSC radical donors/acceptors, so then their hfc constants A_{hfc} obtained experimentally allows determination of the spin density distribution (SDD) in electron donor and acceptor molecules separately. For the most radical ions formed in conjugated polymer:fullerene blends, the hyperfine structure cannot be resolved using the cw EPR technique due to small hfc values and numerous magnetically nonequivalent atoms in organic molecules. While effective magnetic multiresonance methods like electron−nuclear double resonance (ENDOR) and electron nuclear−nuclear triple resonance (TRIPLE) can solve this problem, they are not widely available for routine experiments. However, these methods when combined with quantum chemical calculations (QCC) in most cases are able to define good correlation of the data obtained experimentally and theoretically for undoped and doped conjugated polymers[67−70] as well as for OSC blends.[39,71] Moreover, in many cases where there is a limited number of "magnetic" atoms in the molecular system and suitable ratio of EPR line width and A_{hfc} magnitudes, hfc EPR data could be rather useful and important for the confirmation of QCC results and vice versa. It should be pointed out that for the polymer photoelectron donors, the magnetic resonance technique allows validation of the DFT calculations, in particular, to estimate the delocalization length of the photoinduced polarons formed on polymer chains. Such experiments are important for the estimation of intrinsic quantum efficiency (IQE) of polymers. For instance, precise ENDOR determination of SDD along the oligomer chains has been demonstrated in poly({4,8-bis[(2-ethylhexyl)oxy]benzo-[1,2-*b*:4,5-b′]dithiophene-2,6-diyl}{3-fluoro-2-[(2-ethylhexyl)-carbonyl]thieno[3,4-*b*]thiophenediyl}) (PTB7) and poly[*N*-9″-hepta-decanyl-2,7-carbazole-*alt*-5,5-(4′,7′-di-2-thienyl-2′,1′,3′-benzothiadiazole)] (PCDTBT) polymer photoelectron donors blended with $PC_{71}BM$ as the electron acceptor.[39] The key experimental data obtained demonstrate[39] that ENDOR frequencies of polarons in PTB7and PTDTBT oligomers with different monomers n gives SDD of photoinduced polaron on the polymer chain, i.e., the limit of polaron delocalization expansion due to its coincidence with the ENDOR data in appropriate oligomers. For instance, the information concerning the decrease of polaron delocalization length in PTB7 and PCDTBT in comparison with poly(3-hexylthiophene) (P3HT) correlates with the increase of the short circuit current density (ISC) in OSC that can be attributed, at least partly, to an appropriate increase of the number of photoinduced polarons. Therefore, one of the key directions of study of magnetic resonance application in charge separation

https://doi.org/10.1021/acs.jpcc.1c03427
J. Phys. Chem. C 2021, 125, 12224−12240

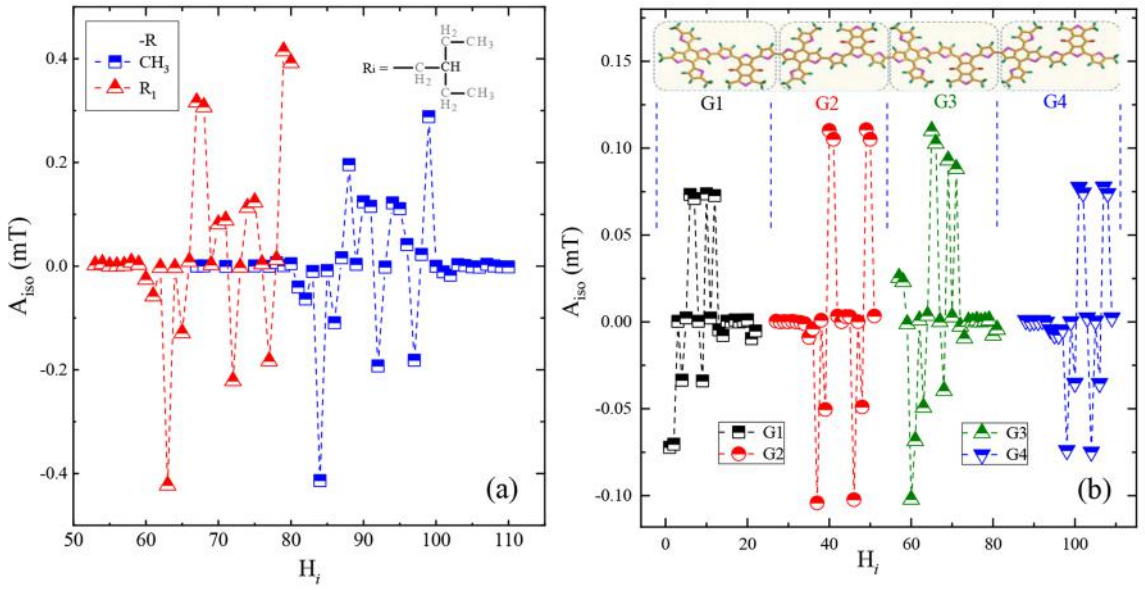

Figure 6. A_{iso} constants of jth hydrogen atoms, H_j, in BDB-T monomers with different side R groups, see Figure 5, n = 1 (a) and in 4-BDB-T oligomer (b). Note that the numbering of ^1H_j in panel a is coincident with that of appropriate PCE structures with different R, exhibited in Supporting Information Section IVa. Such numbering in panel b does not correspond to the real numbering, assigned to the ^1H_j denomination in the 4-BDB-T structure displayed in Supporting Information Section IVb. Here, the numbering axes in panel b reflect only the actual number of ^1H_j in the G_k monomer, and the above format is made only for the convenience of presentation in this Figure, taking in mind that ^1H_j numbering axes do not influence the format of A_{iso} data presentation. The actual ^1H_j atom attribution in the appropriate structures is exhibited in Supporting Information Section IVa.

processes in organic solar cells is connected with the processing of experimental hfc magnetic resonance data and their comparison with QCC ones. We started an SDD evaluation in the PBDB-T polymer using an oligomers approach within the DFT, namely by method/functional/basis sets (DFT/B3LYP/6-311G) in Gaussian-2016 and (DFT/B3LYP/G/6-311G**) in ORCA.[72] The preliminary molecular energy minimization and structure optimization were carried out in Chem3D using the MM2 force field method. Calculated oligomers with n monomers of PBDB-T structured with simplified side chains (designated as R in a PBDB-T monomer) are depicted in Figure 5. The experimental part was carried out at K-band EPR (B_0/ν_e = 860 mT/24 GHz) in liquid dichlorobenzene solution at room temperature. Isotropic EPR spectral parameters (A_{iso}, g_{iso}) essentially simplify spectra processing without loss of information concerning hfc, and in the case of two isotropic spectra overlapping the chance of their separation via spectra fitting is higher than in the X-band. However, around room temperature, one can expect only light-induced EPR response from polymer polarons, but possible radicals of impurities are not excluded as well.

It should be pointed out that in theoretical SDD studies, usually the long side chains of oligomers are often omitted due to the economy of computation time. Actually, in some cases, the tail's size may be comparable with the size of the molecular core; however, it does not include fragments with conjugated bonds and therefore weakly influences the SDD. The latter is partly confirmed by DFT evaluation of $A_{iso}(^1H_i)$ for the monomer with different tails R as shown in Figure 6a. Concerning the experiment, the difference of averaged A_{iso} absolute values is insignificant in our case, which leads to simplifying the structures and tails' length. Therefore, an $A_{iso}(^1H_i)$ evaluation of all other oligomers has been carried out according to the above set. The exemplary 4-BDB-T $A_{iso}(^1H_i)$ computation is presented in Figure 6b and demonstrates an expected and evident decrease at about four times round of hfc absolute magnitude as compared with the 1-BDB-T data displayed in Figure 6a. The summarized data are shown in Figure 7, where an approximation of $A_{iso} = F(n)$ indicates the number of monomers occupied by the polaron on the PBDB-T polymer chain equal 5, namely hfc parameters A_{1iso} and A_{2iso}

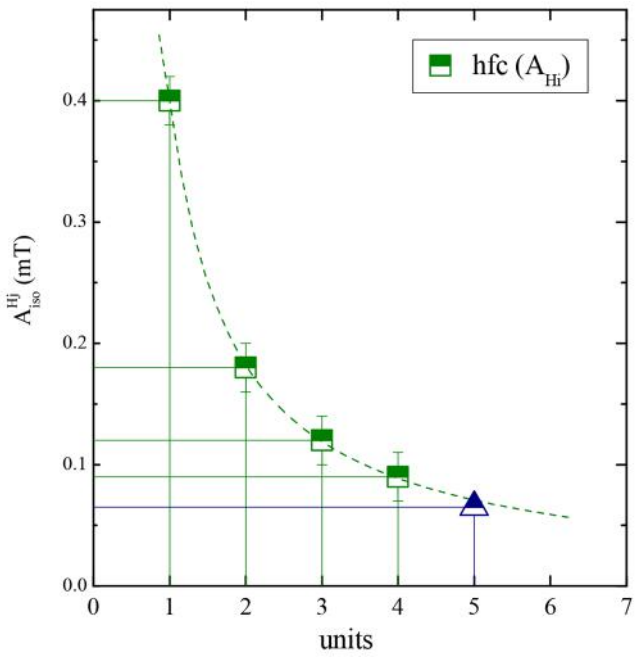

Figure 7. Dependence of the A_{iso} value on the number of chain monomers n occupied by a polaron, equal to 5 for PBDB-T.

https://doi.org/10.1021/acs.jpcc.1c03427
J. Phys. Chem. C 2021, 125, 12224−12240

noted in the caption of Figure 8, obtained by simulation of experimental K-band spectrum shown also in this Figure

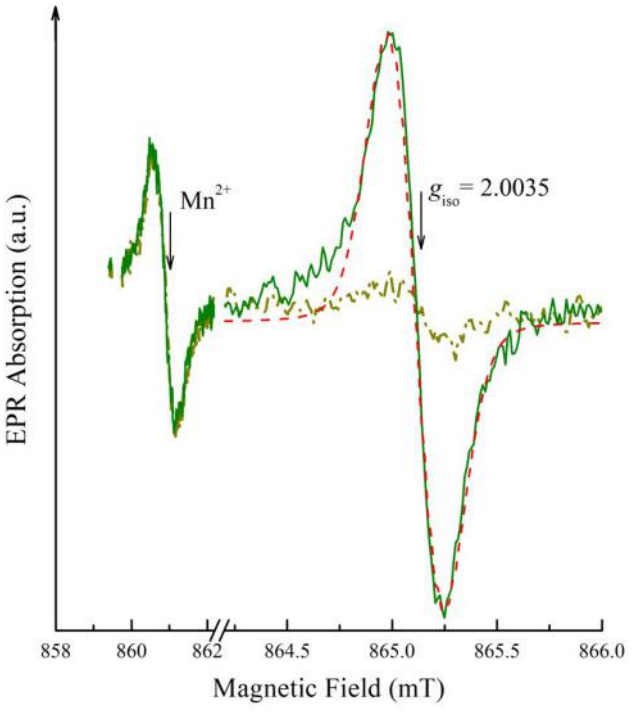

Figure 8. LEPR response of the PBDB-T$^{+\bullet}$ radical photoinitiated in the solution of the PBDB-T:$PC_{61}BM$ composite in dichlorobenzene at T = 294 K. The dark spectrum of this composite is shown by the dash-dotted line. By the dashed line is shown the LEPR spectrum calculated for the hfc structure induced by 11 ^{1}H nuclei with averaged $A_{iso}(^1H_j) \approx 0.065$ mT and 13 ^{1}H with $A_{iso}(^1H_k) \approx 0.035$ mT, and the individual EPR line width used in simulation is $\delta = 0.067 \pm 0.005$ mT. The left situated Mn^{2+} hfc line is the reference line used in K-band for the dark/light spectra coincidence correction.

correlate with those calculated by DFT, namely A_{1iso} is $A_{iso\text{-}ma}$, corresponding to n = 5 in Figure 7. Moreover, the obtained data indicate the essential inhomogeneous broadening of EPR spectra line width due to unresolved hfc structure, and it is taken into account in donor/acceptor spin dynamic consideration by correction coefficient δ ($0.6<\delta<0.7$).

Some preliminary data concerning the possible isomers of ITIC morphology in the view of EPR results are commented on in this section. Magnetic resonance methods are rather sensitive to the local symmetry of the paramagnetic center, resulting in detection of anisotropy in Zeeman and hyperfine interactions in solids. Regarding ITIC, it was noticed that in LEPR experiments, the pronouncedly detected resolved hyperfine structure in EPR spectra has not been found even at the state of radical ion stabilization at a temperature below 80 K. Certainly, it does not indicate the absence of an EPR spectra hyperfine structure, often masked by overlapping of hfc lines. Actually, the evaluated hfc DFT data of ITIC$^{-\bullet}$ with a planar structure (Figure 9a) indicate the good correlation with experimental data, and appropriate data are introduced in Supporting Information Section VI (Figure S12, Table S10). However, the search for possible variants of ITIC isomer morphology by the force field method operated, for instance, in standard MM2 and MMFF94 programs, gave the structure with the steric energy magnitudes less than that for the planar geometry (π-isomer) of ITIC displayed in Figure 9a. The appropriate results attributed to this S-isomer are exhibited in Figure 6b and demonstrate lower A_{0k} values for the monomer and $\pi-\pi$ stacking architecture twice that of the S-isomers as well. Note that we do not have information concerning the direct $\pi-\pi$ stacking morphology formation in PDBT-B:ITIC blends in solid state films and therefore EPR spectra were constructed for planar and S-monomers only. However, calculated isotropic hfc parameters of $\pi-\pi$ stacked dimers displayed in Figure 9 predict the spectra close to monomers and could be considered in details in the above $\pi-\pi$ stacking versions of two and more monomers if necessary. The comparative analysis of experimental and constructed spectra based on S-isomer DFT parameters is summarized in Table S9 and indicates a reasonable coincidence of the experimental and calculated S-isomer versions. The additional data concerning n-$\pi-\pi$ stacking morphology and HOMO/LUMO energy data for both isomers and their oligomers are displayed in the Supporting Information Section V.

3.5. Spin Recombination. When the light is turned off, the spin charge carriers formed as a result of dissociation of photoinitiated excitons in the samples tend to recombine, which leads to a decrease in their concentration. The mechanism and order of such a process should be governed by the structure and morphology of the sample. Recombination of free charge carriers may simply follow the geminate first-order decay order. If a positively charged polaron fast diffusing along the polymer chain does not recombine with the very first oppositely charged counterion, it may collide with a counter radical anion A$^{-\bullet}$ located between copolymer layers. In this case, the charge decay process becomes bimolecular and follows the second order. Assuming that polaron diffusion is not disturbed by the anion molecules, one can conclude that the collision duration is governed by polaron dynamics. The order of charge recombination process m can be evaluated by analyzing the decay of spin concentration $n(t)$ after the light switching off in frame of the trap-limited recombination model:[73]

$$n(t) = n_0(1 + k_r(m-1)n_0^{(m-1)}t)^{1/1-m} \quad (2)$$

where n_0 is the initial number of spin charge carriers at the starting moment of their recombination when t = 0.

A key role in the recombination of spin charge carriers includes spin traps formed in the polymer matrix due to its disordering. Indeed, a captured polaron can either be detrapped by a vacant trap site or recombine with the nearest opposite charge. Multistep trapping and detrapping of a polaron reduces its energy, which results in its more probable localization into a deep spin trap and, therefore, in the increase of concentration of such polarons with time. The charge carriers can recombine during their repeated trapping into and detrapping from a respective position with energetically different depths distributed in a disordered polymer semiconductor. According to such an approach, the decay of charge carriers photoinitiated in a polymer system with energetically different spin traps has to follow the law:[74]

$$n(t) = n_0 + \frac{\pi\xi\delta(1+\xi)\nu_d}{\sin(\pi\xi)}t^{-\xi} \quad (3)$$

where $\xi = k_BT/E_0$, E_0 is the distribution of the energetic depth of a trap, δ is the gamma function, and ν_d is the attempt jump frequency for polaron detrapping. Deconvoluting the sum LEPR spectra, one can register and analyze separately the

https://doi.org/10.1021/acs.jpcc.1c03427
J. Phys. Chem. C 2021, 125, 12224−12240

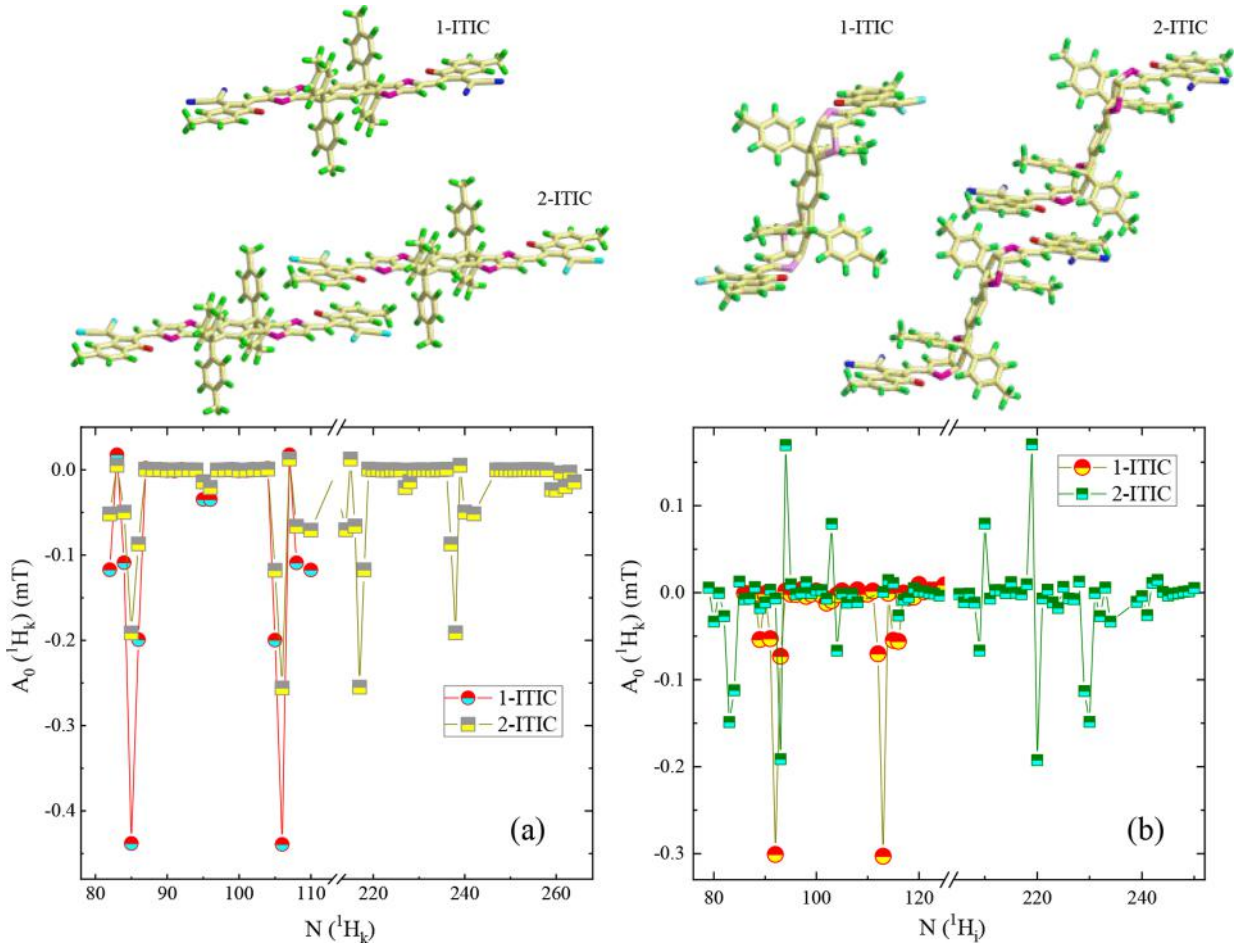

Figure 9. (a) DFT data of all A_0, corresponding to ^1H_K atoms of planar single, 1-ITIC$^{-\bullet}$, and double $\pi-\pi$-stacked, 2-ITIC$^{-\bullet}$, pl-structured radical anions (see Supporting Information Section V). (b) DFT data of all A_0 of ^1H atoms in single, 1-ITIC$^{-\bullet}$, and double, 2-ITIC$^{-\bullet}$, *S*-structured radical anions. ^1H atom numbers coincide with those denominated the appropriate structures in Figures S6 and S8, respectively. The atoms are denominated as follows: cyan, N; yellow, C; red, O; magenta, S; green, H.

decay of effective LEPR susceptibility as well as its contributions due to the mobile and immobilized charge carriers photoinitiated in the polymer system. Figure 10 depicts the decay of the effective LEPR spectra photoinitiated by white light with color temperature T_c = 5000 K in the darkened PBDB-T:$PC_{61}BM$, PBDB-T:$PC_{71}BM$, PBDB-T:ITIC-M, and PBDB-T:ITIC-M/$PPO_{0.06}$ BHJ at T = 77 K. The analysis of the data presented has allowed us to determine from eq 2 the order m of the recombination process occurring in these composites. The data presented in Figure 10 evidence that the decay of charge carriers initiated in these samples follows eq 3 with the respective parameters presented in Table 3. This evidences that this process is carried out in the composites within the framework of the above-mentioned approach. It should be noted that the appearance occurred only after some time in the dependencies shown in Figure 10 of the bell-like component as in the case of other polymer:-fullerene composites.[33,52] Assuming the presumption of formation of an equal quantity of positively and negatively charged carriers upon excitons' dissociation, some reasons for such effect can be proposed. Dissociation of some diamagnetic bipolarons into polaron pairs[61−63] and/or formation in composites of pairs of localized oppositely charged polarons $P^{+\bullet}_{loc}\leftrightarrow P^{-\bullet}_{loc}$ with equal energy and *g*-factors are possible.[60] Spin-dependent and trap-controlled reversible transition $P^{+\bullet}_{loc}\leftrightarrow P^{+\bullet}_{mob}$

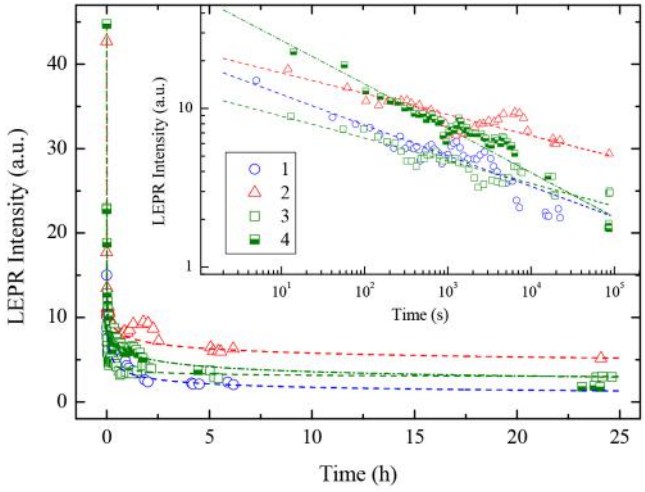

Figure 10. Linear and logarithmic (insert) dependences of the decay of spin charge carriers photoinitiated in the PBDB-T:$PC_{61}BM$ (1), PBDB-T:$PC_{71}BM$ (2), PBDB-T:ITIC-M (3), and PBDB-T:ITIC-M/$PPO_{0.06}$ (4) BHJ by white light with correlation color temperature of T_c = 5000 K at T = 77 K. The lines show the dependences calculated from eq 2 and eq 3 (insert) of the well-fitting experimental data with the appropriate parameters summarized in Table 3.

https://doi.org/10.1021/acs.jpcc.1c03427
J. Phys. Chem. C 2021, 125, 12224−12240

Table 3. Parameters k_r, m[a], n_1, and E_0[b] for Composites with Appropriate Radical Anions at T = 77 K

parameter	$PC_{61}BM^{-\bullet}$	$PC_{71}BM^{-\bullet}$	ITIC-$M^{-\bullet}$	ITIC-$M^{-\bullet}$/$PPO_{0.06}$
k_r, s^{-1}	56.61	3.70	0.020	134.1
m	4.17	7.63	3.85	5.26
n_1	17.99	20.86	12.14	34.10
E_0, eV	0.0343	0.0536	0.0464	0.0301

[a]Obtained from eq 2. [b]Evaluated from eq 3.

can also provoke such dependence.[24] Because m obtained for all samples exceeds two and grows in the series of electron acceptors ITIC-$M^{-\bullet}$ → $PC_{61}BM^{-\bullet}$ → ITIC-$M^{-\bullet}$/PPO → $PC_{71}BM^{-\bullet}$, one could affirm the predominance of the nongeminate recombination process of charge carriers photoexcited in the samples under study. This is accompanied by a tendency increase in the energetic depth E_0 of traps and temperature stability of concentration of spin charge carriers (Figure 10). Therefore, the decay of long-living charge carriers in the samples can successfully be described in terms of the above-mentioned model according to which it is strongly governed by the number, energy depth, and spatial distribution of traps in the polymer matrix.

3.6. Spin Relaxation and Dynamics. Starting from some value of the magnetic component B_1 of the MW field, the effective EPR spectra of the samples change nonlinearly with B_1 due to their MW saturation, as is demonstrated in Figure S5. This nonlinearity depends on different magnetic resonance parameters of paramagnetic centers, especially their electron relaxation. The above-mentioned deconvolution of LEPR spectra of donor−acceptor systems allows to control separately the MW saturation processes of such centers and, thus, to determine their spin−lattice and spin−spin relaxation, which occurs during the respective characteristic times T_1 and T_2. Spin−lattice relaxation is realized when electron spins fall to the ground state as a result of the transfer of their energy to the sample lattice for time T_1 and is determined by the structure, viscosity, polarity, dynamics, *etc.* of the microenvironment of spin ensemble as well as by its precession frequency.[16] Spin−spin relaxation is governed by the hyperfine interaction (hfi) in the surrounding molecular lattice of the electron spins with the nuclei with nonzero spin. These processes are governed mainly by the interaction of charge carriers with their microenvironment and other paramagnetic centers with different spin states and/or spatial distribution.

Figure 11 shows how the T_1 parameter of mobile and immobilized spin charge carriers changes upon their photoinitiation in the samples by photons with different energy $h\nu_{ph}$. The analysis of the data obtained showed a weak dependence of the spin−spin relaxation of the samples on the energy of initiating photons, so their T_2 parameter is not discussed below. It is seen from Figure 11a that the spin−lattice relaxation of localized polarons PBDB-$T^{+\bullet}_{loc}$ and mobile methanofullerene radical anions $PC_{61}BM^{-\bullet}_{mob}$ accelerates monotonically with the increase of the energy of initiating photons $h\nu_{ph}$. At the same time, localized charge carriers $PC_{61}BM^{-\bullet}_{loc}$ demonstrate an extreme dependence of $T_1(h\nu_{ph})$ with an extremum at $h\nu_{ph}$ = 1.75 eV which changes weakly at $h\nu_{ph} \geq 2.2$ eV. Analogous energy independence was registered in the study of spin charge carriers excited in $PC_{71}BM$-modified P3DDT by photons with the energy of $h\nu_{ph}$ = 2.10 eV.[50] Once the molecules $PC_{61}BM$ in the composite under study are replaced by the $PC_{71}BM$ ones, its dependence $T_1(h\nu_{ph})$ becomes weaker (Figure 11b). The same tendency is noticed for spin−lattice relaxation of radical anions immobilized in the composite PBDB-T:ITIC-M (Figure 11c). On the other hand, such dependences obtained for localized polarons PBDB-$T^{+\bullet}_{loc}$ and pairs of mobile charge carriers PBDB-$T^{+\bullet}_{mob}$ ↔ ITIC-$M^{+\bullet}_{mob}$ are characterized by at least one extremum at 1.79 and 1.62 eV, respectively (Figure 11c). Such sensitivity of electron relaxation to the energy of the light photons can be attributed to the intrinsic band structure of the composite matrix. It should be noted that the weak doping of this composite with the PPO molecules leads to a shift of these extremes to 2.01 and 2.08 eV, respectively (Figure 11c). The

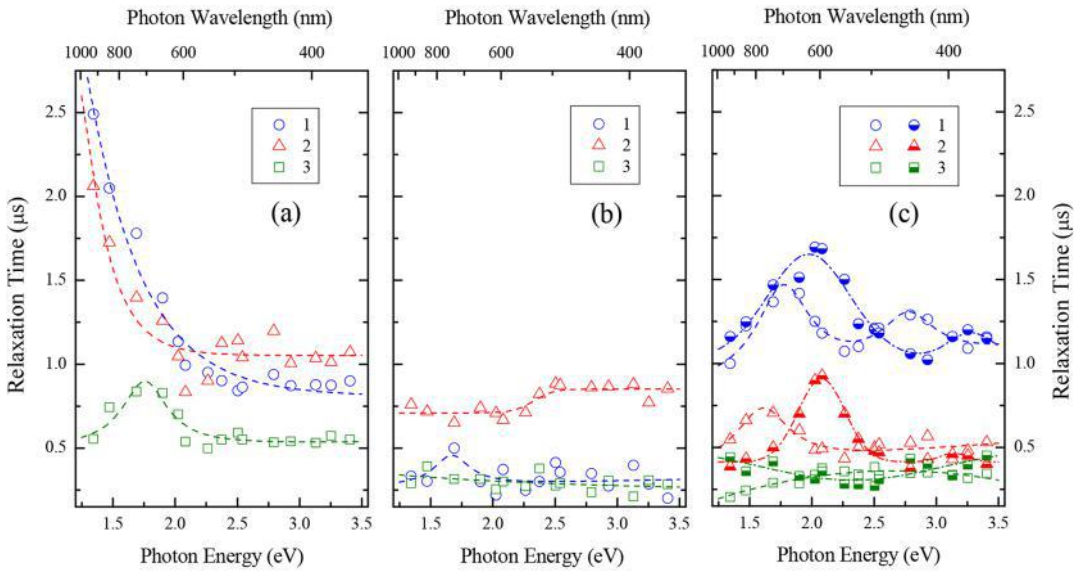

Figure 11. Spin−lattice relaxation time of charge carriers PBDB-$T^{+\bullet}_{loc}$ (1), $A^{-\bullet}_{mob}$(2), and $A^{-\bullet}_{loc}$(3) background excited in the PBDB-T:$PC_{61}BM$ (a), PBDB-T:$PC_{71}BM$ (b), PBDB-T:ITIC-M (c, open points), and PBDB-T:ITIC-M/$PPO_{0.06}$ (c, semifilled points) composites at T = 77 K as function of the photon frequency/wavelength, $h\nu_{ph}/\lambda_{ph}$. The lines are drawn arbitrarily only for illustration to guide the eye.

https://doi.org/10.1021/acs.jpcc.1c03427
J. Phys. Chem. C 2021, 125, 12224−12240

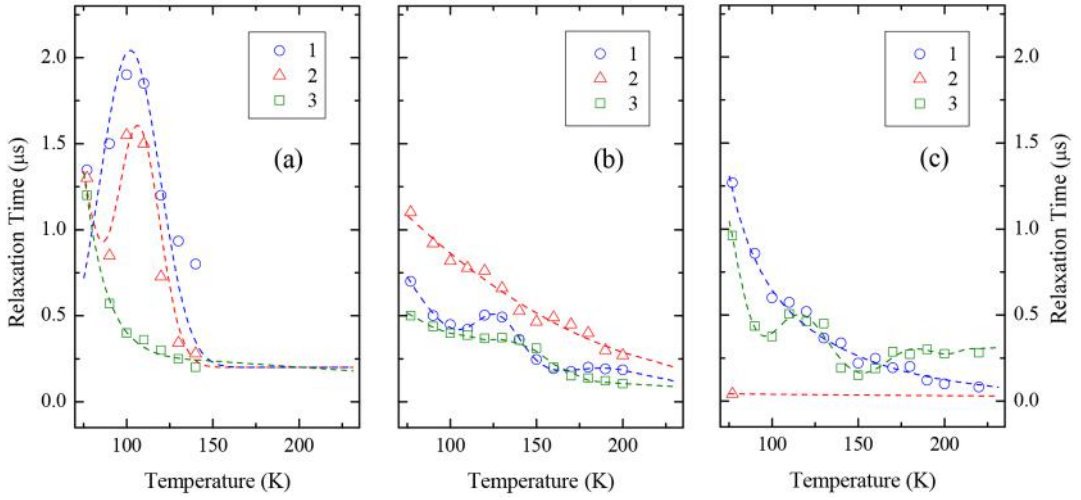

Figure 12. Temperature dependences of spin−lattice relaxation time of charge carriers PBDB-$T^{+\bullet}_{loc}$ (1), $A^{-\bullet}_{mob}$(2), and $A^{-\bullet}_{loc}$(3) background excited by white light with correlation color temperature of T_c = 5000 K in the PBDB-T:$PC_{61}BM$ (a), PBDB-T:$PC_{71}BM$ (b), and PBDB-T:ITIC-M (c) composites. The lines are drawn arbitrarily only for illustration to guide the eye.

latter circumstance may indicate, e.g., more lamellar morphology of the PPO-modified composite.

Electron relaxation of the spin carrier charges is also governed by their interaction with the phonons of a microenvironmental lattice. Figure 12 shows the temperature dependences of the spin−lattice relaxation time of charge carriers photoinitiated in the PBDB-T-based BHJ by photons of white light with the column temperature of T_c = 5000 K. From the analysis of the data presented, some basic conclusions can be made. The first of them is an expected trivial acceleration of such relaxation with heating of the samples. More important is the appearance of the extreme terms on the temperature dependences of polarons captured by traps in the PBDB-T:$PC_{61}BM$ and PBDB-T:$PC_{71}BM$ backbones, radical anions immobilized in the PBDB-T:ITIC-M BHJ, as well as of mobile charge carrier pairs in the composite PBDB-T:$PC_{61}BM$. The characteristic position of these terms varies within the region of ca. T = 105−130 K depending on the basic composite properties. Such effect can be attributed, e.g., to the above-mentioned possible transition of some diamagnetic bipolarons to spin polaron pairs. Such transition should reinforce an effective spin exchange coupling and provoke temperature dependences similar to those shown in Figure 4. Because the rate of quasi-one-dimensional diffusion of N_P polarons along polymer chains depends on their spin−lattice relaxation time T_1 as $\nu^P_{1D} \propto N_P^2 T_1^2$,[28,75] one can expect a complex change of their dynamics parameters with the temperature. Finally, a sufficient acceleration of spin−lattice relaxation and the reduction of the concentration of mobile charge carriers when heated the PBDB-T:ITIC-M BHJ should be noted (see Figure 12c). It confirms the above-mentioned significant increase in the exchange $\pi-\pi$-interaction of spin charge carriers situated on the nearest lamellar microenvironment. Polaron confinement blocks intrachain diffusion of the charge and accelerates recombination and interlayer charge hopping. Optimal modification of the sample with the small planar molecules additionally orders the composite matrix. As a result, the charge is transferred most quickly through its neighboring planes, which predetermines the better efficiency and functionality of such a composite.

CONCLUSION

The results obtained demonstrate the advantages of the cw LEPR spectroscopy in the study of dynamics, relaxation, recombination, and other spin-assisted processes occurring in organic polymer composites. Light irradiation of PBDB-T-based composites with different dimensional electron acceptors was shown to provoke the appearance in their BHJ of spin polarons and appropriate radical anions, the concentration and magnetic resonant parameters of which are governed by their structural and energetic properties. Some charge carriers are captured by spin traps forming in polymer matrixes due to their disordering, which exhibits a weak anisotropy of their magnetic resonant parameters. Along with mobile charge carriers, trapped carriers also participate in charge transfer through BHJ of composites, but indirectly. The distribution of the density and energetic depth of spin traps are governed by the structural, conformational, and other properties of the composite matrixes. These parameters change significantly when the composite replaced the counterion and/or is modified with suitable small 2D molecules. This enhances the $\pi-\pi$-interaction of polarons formed on its neighboring chains and reduces the probability of their recombination with the nearest counterions. As a result, this shifts the equilibrium of the processes of formation and recombination, thereby increasing the stability of spin charge carriers and their LEPR signals. Ultimately, the concentration of all spin charge carriers increases by more than an order of magnitude in the series of composites PBDB-T:$PC_{61}BM$ → PBDB-T:ITIC-M → PBDB-T:ITIC-M/$PPO_{0.06}$ → PBDB-T:$PC_{71}BM$. This correlates positively with the number of light quanta absorbed by their BHJ and negatively with the respective energy bandgap. The interaction of spins differently situated in the bandgap provokes an extreme photon energy sensitivity of the spin-assisted processes carried out in the polymer composites under study. Molecular and band structures of these systems were also shown to significantly influence electron relaxation of charge carriers, which is governed by the exchange interaction of their spin carriers with their microenvironment, phonons of the polymer matrix, and exciting light photons. Polaron delocalization along the PBDB-T chain corresponding to 4−5 monomers has been evaluated by DFT and K-band EPR

https://doi.org/10.1021/acs.jpcc.1c03427
J. Phys. Chem. C 2021, 125, 12224−12240

technique. Inhomogeneous EPR line broadening due to unresolved ^{1}H hfc has been estimated by LEPR spectra simulation based on DFT data, resulting in the coefficient of line width correction to be equal to about 0.6−0.7. Predominant nongeminate recombination of long-living charge carriers can be described in terms of their multistep trapping−detrapping hopping between sites of the polymer matrix. It is strongly governed by the number, energy depth, and spatial distribution of spin traps and controls the stability of photoinitiated charge carriers. $\pi-\pi$-Coupling of polarons excited in neighboring polymer chains increases as the methanofullerene counterions are replaced by lower-dimensional ITIC-M ones and grows continuously at slight doping of the composite with small planar PPO molecules with an extended π-system. This provokes higher polaron confinement, blocks intrachain free charge diffusion, and accelerates charge hopping through the layers of the nonfullerene polymer composite.

■ ASSOCIATED CONTENT

Supporting Information

The Supporting Information is available free of charge at https://pubs.acs.org/doi/10.1021/acs.jpcc.1c03427.

Section I, NIR-vis-UV spectra of the samples; Section II, LED sources used in experiments; Section III, spin−lattice relaxation of charge carriers in PBDB-based composites; Section IV, structure and HFC parameters ($A_{iso} = A_0$) of monomer 1-BDB-T; Section V, structure and HFC parameters ($A_{iso} = A_0$) of single 1-ITIC-pl and double 2-ITIC-pl; Section VI, processing of the experimental spectrum of the ITIC:PBDB-T composite (PDF)

■ AUTHOR INFORMATION

Corresponding Author

Victor I. Krinichnyi − *Department of Kinetics and Catalysis, Institute of Problems of Chemical Physics RAS, Chernogolovka 142432, Russia;* orcid.org/0000-0002-5227-763X; Phone: +7(496-52) 21882; Email: kivirus@gmail.com

Authors

Evgeniya I. Yudanova − *Department of Kinetics and Catalysis, Institute of Problems of Chemical Physics RAS, Chernogolovka 142432, Russia*

Nikolay N. Denisov − *Department of Kinetics and Catalysis, Institute of Problems of Chemical Physics RAS, Chernogolovka 142432, Russia*

Aleksei A. Konkin − *Center for Micro- and Nanotechnologies, Ilmenau University of Technology, D-98693 Ilmenau, Germany; Institute of Physics, Kazan Federal University, 420008 Kazan, Russia*

Uwe Ritter − *Center for Micro- and Nanotechnologies, Ilmenau University of Technology, D-98693 Ilmenau, Germany;* orcid.org/0000-0002-9315-4863

Victor R. Bogatyrenko − *Department of Kinetics and Catalysis, Institute of Problems of Chemical Physics RAS, Chernogolovka 142432, Russia*

Alexander L. Konkin − *Center for Micro- and Nanotechnologies, Ilmenau University of Technology, D-98693 Ilmenau, Germany;* orcid.org/0000-0002-2418-2676

Complete contact information is available at: https://pubs.acs.org/10.1021/acs.jpcc.1c03427

Notes

The authors declare no competing financial interest.

■ ACKNOWLEDGMENTS

This work was performed with financial support from the Russian Foundation for Basic Research, Grant No. 18-29-20011-mk according to the State Assignment, No. AAAA-A19-119032690060-9, and was partly supported by the Russian Government Program of Competitive Growth of Kazan Federal University.

■ REFERENCES

(1) Li, G.; Zhu, R.; Yang, Y. Polymer Solar Cells. *Nat. Photonics* **2012**, *6*, 153−161.

(2) Lu, L.; Zheng, T.; Wu, Q.; Schneider, A. M.; Zhao, D.; Yu, L. Recent Advances in Bulk Heterojunction Polymer Solar Cells. *Chem. Rev.* **2015**, *115*, 12666−12731.

(3) Yao, H.; Ye, L.; Zhang, H.; Li, S.; Zhang, S.; Hou, J. Molecular Design of Benzodithiophene-Based Organic Photovoltaic Materials. *Chem. Rev.* **2016**, *116*, 7397−7457.

(4) Holliday, S. *Synthesis and Characterisation of Non-Fullerene Electron Acceptors for Organic Photovoltaics*; Springer, 2018.

(5) Lin, Y.; Wang, J.; Zhang, Z.-G.; Bai, H.; Li, Y.; Zhu, D.; Zhan, X. An Electron Acceptor Challenging Fullerenes for Efficient Polymer Solar Cells. *Adv. Mater.* **2015**, *27*, 1170−1174.

(6) Li, S.; Ye, L.; Zhao, W.; Zhang, S.; Mukherjee, S.; Ade, H.; Hou, J. Energy-Level Modulation of Small-Molecule Electron Acceptors to Achieve over 12% Efficiency in Polymer Solar Cells. *Adv. Mater.* **2016**, *28*, 9423−9429.

(7) An, Q.; Zhang, F.; Gao, W.; Sun, Q.; Zhang, M.; Yang, C.; Zhang, J. High-Efficiency and Air Stable Fullerene-Free Ternary Organic Solar Cells. *Nano Energy* **2018**, *45*, 177−183.

(8) Zhang, G.; Chen, X.-K.; Xiao, J.; Chow, P. C. Y.; Ren, M.; Kupgan, G.; Jiao, X.; Chan, C. C. S.; Du, X.; Xia, R.; et al. Delocalization of Exciton and Electron Wavefunction in Non-Fullerene Acceptor Molecules Enables Efficient Organic Solar Cells. *Nat. Commun.* **2020**, *11*, 3943.

(9) Zhao, W.; Li, S.; Zhang, S.; Liu, X.; Hou, J. Ternary Polymer Solar Cells Based on Two Acceptors and One Donor for Achieving 12.2% Efficiency. *Adv. Mater.* **2017**, *29*, 1604059.

(10) Zhao, W.; Qian, D.; Zhang, S.; Li, S.; Inganäs, O.; Gao, F.; Hou, J. Fullerene-Free Polymer Solar Cells with over 11% Efficiency and Excellent Thermal Stability. *Adv. Mater.* **2016**, *28*, 4734−4739.

(11) Cui, Y.; Yao, H.; Gao, B.; Qin, Y.; Zhang, S.; Yang, B.; He, C.; Xu, B.; Hou, J. Fine-Tuned Photoactive and Interconnection Layers for Achieving over 13% Efficiency in a Fullerene-Free Tandem Organic Solar Cell. *J. Am. Chem. Soc.* **2017**, *139*, 7302−7309.

(12) Yang, F.; Li, C.; Lai, W.; Zhang, A.; Huang, H.; Li, W. Halogenated Conjugated Molecules for Ambipolar Field-Effect Transistors and Non-Fullerene Organic Solar Cells. *Mater. Chem.y Fron.* **2017**, *1*, 1389−1395.

(13) Park, Y.; Fuentes-Hernandez, C.; Jia, X.; Larrain, F. A.; Zhang, J.; Marder, S. R.; Kippelen, B. Measurements of the Field-Effect Electron Mobility of the Acceptor ITIC. *Org. Electron.* **2018**, *58*, 290−293.

(14) Wen, S.; Chen, W.; Huang, G.; Shen, W.; Liu, H.; Duan, L.; Zhang, J.; Yang, R. 2d Expanded Conjugated Polymers with Non-Fullerene Acceptors for Efficient Polymer Solar Cells. *J. Mater. Chem. C* **2018**, *6*, 1753−1758.

(15) Krinichnyi, V. I.; Yudanova, E. I.; Bogatyrenko, V. R. Effect of Spin Localization on Charge Transport in Low-Bandgap Bilayered Ordered Nanocomposites. *Sol. Energy Mater. Sol. Cells* **2018**, *174*, 333−341.

(16) Misra, S. K. *Multifrequency Electron Paramagnetic Resonance. Theory and Applications.*; Wiley-VCH: Weinheim, 2011; p 1056.
(17) Krinichnyi, V. I. *Multi Frequency EPR Spectroscopy of Conjugated Polymers and Their Nanocomposites*; CRC Press Taylor & Francis Group: Boca Raton, FL, 2016.
(18) Naveed, K.-u.-R.; Wang, L.; Yu, H.; Ullah, R. S.; Haroon, M.; Fahad, S.; Li, J.; Elshaarani, T.; Khan, R. U.; Nazir, A. Recent Progress in the Electron Paramagnetic Resonance Study of Polymers. *Polym. Chem.* **2018**, *9*, 3306−3335.
(19) Krinichnyi, V. I. EPR Spectroscopy of Polymer:Fullerene Nanocomposites. In *Spectroscopy of Polymer Nanocomposites*, 1st ed.; Thomas, S., Rouxel, D., Ponnamma, D., Eds.; Elsevier: Amsterdam, 2016; pp 202−275.
(20) Niklas, J.; Poluektov, O. G. Charge Transfer Processes in OPV Materials as Revealed by EPR Spectroscopy. *Adv. Energy Mater.* **2017**, *7*, 1602226.
(21) Krinichnyi, V. I.; Yudanova, E. I.; Denisov, N. N.; Bogatyrenko, V. R. Light-Induced Electron Paramagnetic Resonance Spectroscopy of Spin-Assisted Charge Transfer in Narrow-Bandgap Copolymer:-Methanofullerene Composites. *J. Phys. Chem. C* **2019**, *123*, 16533−16545.
(22) Krinichnyi, V. I.; Yudanova, E. I.; Denisov, N. N.; Konkin, A. A.; Ritter, U.; Wessling, B.; Konkin, A.; Bogatyrenko, V. R. Impact of Spin-Exchange Interaction on Charge Transfer in Dual-Polymer Photovoltaic Composites. *J. Phys. Chem. C* **2020**, *124*, 10852−10869.
(23) Kraffert, F.; Steyrleuthner, R.; Albrecht, S.; Neher, D.; Scharber, M. C.; Bittl, R.; Behrends, J. Charge Separation in PCDTBT:PCBM Blends from an EPR Perspective. *J. Phys. Chem. C* **2014**, *118*, 28482−28493.
(24) Zhao, F. G.; Wang, K.; Duan, J. S.; Zhu, X. X.; Lu, K.; Zhao, C. G.; Zhang, C. X.; Yu, H. M.; Hu, B. Spin-Dependent Electron-Hole Recombination and Dissociation in Nonfullerene Acceptor ITIC-Based Organic Photovoltaic Systems. *Solar RRL* **2019**, *3*, 1900063.
(25) Van Landeghem, M.; Maes, W.; Goovaerts, E.; Van Doorslaer, S. Disentangling Overlapping High-Field EPR Spectra of Organic Radicals: Identification of Light-Induced Polarons in the Record Fullerene-Free Solar Cell Blend PBDB-T:ITIC. *J. Magn. Reson.* **2018**, *288*, 1−10.
(26) Davidov, D.; Moraes, F.; Heeger, A. J.; Wudl, F.; Kim, H.; Dalton, L. R. Electron-Spin Echo Modulation and Relaxation in Polythiophene. *Solid State Commun.* **1985**, *53*, 497−500.
(27) Mizoguchi, K. Spin Dynamics Study in Conducting Polymers by Magnetic-Resonance. *Jpn. J. Appl. Phys. Part 1* **1995**, *34*, 1−19.
(28) Mizoguchi, K.; Kuroda, S. Magnetic Properties of Conducting Polymers. In *Handbook of Organic Conductive Molecules and Polymers*; Nalwa, H. S., Ed.; John Wiley & Sons: Chichester, NY, 1997; Vol. 3, pp 251−317.
(29) Uvarov, M. N.; Kulik, L. V. Electron Spin Echo of Photoinduced Spin-Correlated Polaron Pairs in P3HT:PCBM Composite. *Appl. Magn. Reson.* **2013**, *44*, 97−106.
(30) Williams, J. M.; Ferraro, J. R.; Thorn, R. J.; Carlson, K. D.; Geiser, U.; Wang, H. H.; Kini, A. M.; Whangboo, M. H. *Organic Superconductors (Including Fullerenes): Synthesis, Structure, Properties, and Theory*; Prentice-Hall, Inc.: Englewood Cliffs, New Jersey, 1992.
(31) Lu, X. H.; Hlaing, H.; Germack, D. S.; Peet, J.; Jo, W. H.; Andrienko, D.; Kremer, K.; Ocko, B. M. Bilayer Order in a Polycarbazole-Conjugated Polymer. *Nat. Commun.* **2012**, *3*, 1290.
(32) Ermolaev, G. A.; Grudinin, D. V.; Stebunov, Y. V.; Voronin, K. V.; Kravets, V. G.; Duan, J.; Mazitov, A. B.; Tselikov, G. I.; Bylinkin, A.; Yakubovsky, D. I.; et al. Giant Optical Anisotropy in Transition Metal Dichalcogenides for Next-Generation Photonics. *Nat. Commun.* **2021**, *12*, 854.
(33) Krinichnyi, V. I.; Yudanova, E. I.; Denisov, N. N.; Bogatyrenko, V. R. Effects of Small-Molecule-Doping on Spin-Assisted Processes in P3DDT:$PC_{61}BM$ Photovoltaics. *Synth. Met.* **2020**, *267*, 116462.
(34) Al Ibrahim, M.; Roth, H.-K.; Schrödner, M.; Konkin, A.; Zhokhavets, U.; Gobsch, G.; Scharff, P.; Sensfuss, S. The Influence of the Optoelectronic Properties of Poly(3-Alkylthiophenes) on the Device Parameters in Flexible Polymer Solar Cells. *Org. Electron.* **2005**, *6*, 65−77.
(35) Huh, Y. H.; Park, B. Interface-Engineering Additives of Poly(Oxyethylene Tridecyl Ether) for Low-Band Gap Polymer Solar Cells Consisting of PCDTBT:PCBM70 Bulk-Heterojunction Layers. *Opt. Express* **2013**, *21*, A146−A156.
(36) Mohankumar, S.; Kannaian, T.; Sathyanarayanamoorthi, V. The Effect of Substituted 2,5-Diphenyloxazole on DSSC Performance: A Theoretical Study. *Int. J. Adv. Res. Dev.* **2018**, *3*, 1154−1159.
(37) Konkin, A.; Ritter, U.; Scharff, P.; Roth, H.-K.; Aganov, A.; Sariciftci, N. S.; Egbe, D. A. M. Photo-Induced Charge Separation Process in (PCBM-$C_{120}O$)/(M3EH-PPV) Blend Solid Film Studied by Means of X- and K-Bands ESR at 77 and 120 K. *Synth. Met.* **2010**, *160*, 485−489.
(38) Poluektov, O. G.; Filippone, S.; Martín, N.; Sperlich, A.; Deibel, C.; Dyakonov, V. Spin Signatures of Photogenerated Radical Anions in Polymer-[70]Fullerene Bulk Heterojunctions: High Frequency Pulsed EPR Spectroscopy. *J. Phys. Chem. B* **2010**, *114*, 14426−14429.
(39) Niklas, J.; Mardis, K. L.; Banks, B. P.; Grooms, G. M.; Sperlich, A.; Dyakonov, V.; Beaupré, S.; Leclerc, M.; Xu, T.; Yue, L.; et al. Highly-Efficient Charge Separation and Polaron Delocalization in Polymer−Fullerene Bulk-Heterojunctions: A Comparative Multi-Frequency EPR and DFT Study. *Phys. Chem. Chem. Phys.* **2013**, *15*, 9562−9574.
(40) Krzystek, J.; Sienkiewicz, A.; Pardi, L.; Brunel, L. C. DPPH as a Standard for High-Field EPR. *J. Magn. Reson.* **1997**, *125*, 207−211.
(41) Stoll, S.; Schweiger, A. EasySpin, a Comprehensive Software Package for Spectral Simulation and Analysis in EPR. *J. Magn. Reson.* **2006**, *178*, 42−55.
(42) Weil, J. A.; Bolton, J. R.; Wertz, J. E. *Electron Paramagnetic Resonance: Elementary Theory and Practical Applications*; Wiley-Interscience: New York, 2007; Vol. *2d*.
(43) Marumoto, K.; Takeuchi, N.; Ozaki, T.; Kuroda, S. ESR Studies of Photogenerated Polarons in Regioregular Poly(3-Alkylthiophene)-Fullerene Composite. *Synth. Met.* **2002**, *129*, 239−247.
(44) Bin, H.; Zhang, Z.-G.; Gao, L.; Chen, S.; Zhong, L.; Xue, L.; Yang, C.; Li, Y. Non-Fullerene Polymer Solar Cells Based on Alkylthio and Fluorine Substituted 2D-Conjugated Polymers Reach 9.5% Efficiency. *J. Am. Chem. Soc.* **2016**, *138*, 4657−4664.
(45) Hare, J. P.; Kroto, H. W.; Taylor, R. Preparation and UV/Visible Spectra of Fullerenes C60 and C70. *Chem. Phys. Lett.* **1991**, *177*, 394−398.
(46) Huang, J. H.; Lee, C. P.; Ho, Z. Y.; Kekuda, D.; Chu, C. W.; Ho, K. C. Enhanced Spectral Response in Polymer Bulk Heterojunction Solar Cells by Using Active Materials with Complementary Spectra. *Sol. Energy Mater. Sol. Cells* **2010**, *94*, 22−28.
(47) Berliner, L. J. *Spin Labeling I: Theory and Application*; Academic Press: New York, 1976; Vol. *1*, p 592.
(48) Likhtenshtein, G. I. *Electron Spin Interactions in Chemistry and Biology: Fundamentals, Methods, Reactions Mechanisms, Magnetic Phenomena, Structure Investigation*; Springer, 2016.
(49) Konkin, A.; Ritter, U.; Konkin, A. A.; Mamin, G.; Orlinskii, S.; Gafurov, M.; Aganov, A.; Klochkov, V.; Lohwasser, R.; Thelakkat, M.; et al. W-Band ENDOR of Light-Induced PPerAcr Anion Radicals in Double-Crystalline Donor−Bridge−Acceptor P3HT-b-PPerAcr Block Copolymer in Frozen Solution: Experimental and DFT Study. *J. Phys. Chem. C* **2018**, *122*, 22829−22837.
(50) Krinichnyi, V. I.; Yudanova, E. I. Light-Induced EPR Study of Charge Transfer in P3HT/$PC_{71}BM$ Bulk Heterojunctions. *J. Phys. Chem. C* **2012**, *116*, 9189−9195.
(51) Krinichnyi, V. I.; Yudanova, E. I. Influence of Morphology of Low-Band-Gap PCDTBT:$PC_{71}BM$ Composite on Photoinduced Charge Transfer: LEPR Spectroscopy Study. *Synth. Met.* **2015**, *210*, 148−155.
(52) Krinichnyi, V. I.; Yudanova, E. I.; Bogatyrenko, V. R. Light-Induced EPR Study of Spin-Assisted Charge Transport in PFOT:$PC_{61}BM$ Composite. *J. Photochem. Photobiol., A* **2019**, *372*, 288−295.

https://doi.org/10.1021/acs.jpcc.1c03427
J. Phys. Chem. C 2021, 125, 12224−12240

(53) Cho, S.; Kim, S.; Kim, J.; Jo, Y.; Ryu, I.; Hong, S.; Lee, J.-J.; Cha, S.; Nam, E. B.; Lee, S. U.; et al. Hybridisation of Perovskite Nanocrystals with Organic Molecules for Highly Efficient Liquid Scintillators. *Light: Sci. Appl.* **2020**, *9*, 156.
(54) Nelson, J. Diffusion-Limited Recombination in Polymer-Fullerene Blends and Its Influence on Photocurrent Collection. *Phys. Rev. B: Condens. Matter Mater. Phys.* **2003**, *67*, 155209.
(55) Molin, Y. N.; Salikhov, K. M.; Zamaraev, K. I. *Spin Exchange: Principles and Applications in Chemistry and Biology*; Springer-Verlag: Berlin Heidelberg, 1980; Vol. *8*.
(56) Houze, E.; Nechtschein, M. ESR in Conducting Polymers: Oxygen-Induced Contribution to the Linewidth. *Phys. Rev. B: Condens. Matter Mater. Phys.* **1996**, *53*, 14309−14318.
(57) Krinichnyi, V. I.; Yudanova, E. I.; Spitsina, N. G. Light-Induced EPR Study of Poly(3-Alkylthiophene)/Fullerene Composites. *J. Phys. Chem. C* **2010**, *114*, 16756−16766.
(58) Krinichnyi, V. I.; Yudanova, E. I. Structural Effect of Electron Acceptor on Charge Transfer in Poly(3-Hexylthiophene)/Methanofullerene Bulk Heterojunctions. *Sol. Energy Mater. Sol. Cells* **2011**, *95*, 2302−2313.
(59) Krinichnyi, V. I. Dynamics of Spin Charge Carriers in Polyaniline. *Appl. Phys. Rev.* **2014**, *1*, 021305.
(60) Dyakonov, V.; Zoriniants, G.; Scharber, M.; Brabec, C. J.; Janssen, R. A. J.; Hummelen, J. C.; Sariciftci, N. S. Photoinduced Charge Carriers in Conjugated Polymer-Fullerene Composites Studied with Light-Induced Electron-Spin Resonance. *Phys. Rev. B: Condens. Matter Mater. Phys.* **1999**, *59*, 8019−8025.
(61) Kaufman, J. H.; Colaneri, N.; Scott, J. C.; Street, G. B. Evolution of Polaron States into Bipolarons in Polypyrrole. *Phys. Rev. Lett.* **1984**, *53*, 1005−1008.
(62) Čík, G.; Šeršeň, F.; Dlháň, L. Thermally Induced Transitions of Polarons to Bipolarons in Poly (3-Dodecylthiophene). *Synth. Met.* **2005**, *151*, 124−130.
(63) Baleg, A. A.; Masikini, M.; John, S. V.; Williams, A. R.; Jahed, N.; Baker, P.; Iwuoha, E. Conducting Polymers and Composites. In *Functional Polymers*; Mazumder, M. J., Sheardown, H., Al-Ahmed, A., Eds.; Springer: Cham, 2019; pp 1−54.
(64) Matos-Abiague, A. A Fractional-Dimensional Space Approach to the Polaron Effect in Quantum Wells. *J. Phys.: Condens. Matter* **2002**, *14*, 4543−4552.
(65) Pinheiro, C. D.; Silva, G. M. E. Dynamics of Polarons and Bipolarons with Interchain Coupling in Conjugated Polymers. *Int. J. Quantum Chem.* **2003**, *95*, 153−158.
(66) Denti, I.; Cimò, S.; Brambilla, L.; Milani, A.; Bertarelli, C.; Tommasini, M.; Castiglioni, C. Polaron Confinement in N-Doped P(NDI2OD-T2) Unveiled by Vibrational Spectroscopy. *Chem. Mater.* **2019**, *31*, 6726−6739.
(67) Kuroda, S.; Noguchi, T.; Ohnishi, T. Electron-Nuclear Double-Resonance Observation of π-Electron Direct States in Undoped Poly(para-Phenylene Vinylene). *Phys. Rev. Lett.* **1994**, *72*, 286−289.
(68) Kuroda, S.; Noguchi, T.; Ohnishi, T. ENDOR Spectroscopy of Poly(para-Phenylene Vinylene). *Synth. Met.* **1995**, *69*, 423−424.
(69) Kuroda, S. ESR and ENDOR studies of solitons and polarons in conjugated polymers. *Appl. Magn. Reson.* **2003**, *23*, 455−468.
(70) Aguirre, A.; Gast, P.; Orlinskii, S.; Akimoto, I.; Groenen, E. J. J.; El Mkami, H.; Goovaerts, E.; Van Doorslaer, S. Multifrequency EPR Analysis of the Positive Polaron in I_2-Doped Poly(3-Hexylthiophene) and in Poly[2-Methoxy-5-(3,7-Dimethyloctyloxy)]-1,4-Phenylenevinylene. *Phys. Chem. Chem. Phys.* **2008**, *10*, 7129−7138.
(71) Marumoto, K.; Kato, M.; Kondo, H.; Kuroda, S.; Greenham, N. C.; Friend, R. H.; Shimoi, Y.; Abe, S. Electron Spin Resonance and Electron Nuclear Double Resonance of Photogenerated Polarons in Polyfluorene and Its Fullerene Composite. *Phys. Rev. B: Condens. Matter Mater. Phys.* **2009**, *79*, 245204.
(72) Neese, F. The ORCA Program System. *Wiley Interdiscip. Rev.: Comput. Mol. Sci.* **2012**, *2*, 73−78.
(73) Lukina, E. A.; Uvarov, M. N.; Kulik, L. V. Charge Recombination in P3HT/PC70BM Composite Studied by Light-Induced EPR. *J. Phys. Chem. C* **2014**, *118*, 18307−18314.
(74) Tachiya, M.; Seki, K. Theory of Bulk Electron-Hole Recombination in a Medium with Energetic Disorder. *Phys. Rev. B: Condens. Matter Mater. Phys.* **2010**, *82*, 085201.
(75) Nechtschein, M. Electron Spin Dynamics. In *Handbook of Conducting Polymers*; Skotheim, T. A., Elsenbaumer, R. L., Reynolds, J. R., Eds.; Marcel Dekker: New York, 1997; pp 141−163.

https://doi.org/10.1021/acs.jpcc.1c03427
J. Phys. Chem. C 2021, 125, 12224−12240